JGR Biogeosciences

RESEARCH ARTICLE
10.1029/2022JG006823

Whiting Events in a Large Peri-Alpine Lake: Evidence of a Catchment-Scale Process

Nicolas Escoffier[1], Pascal Perolo[1], Thibault Lambert[1], Janine Rüegg[1,2], Daniel Odermatt[3], Thierry Adatte[4], Torsten Vennemann[1], and Marie-Elodie Perga[1]

[1]Institute of Earth Surface Dynamics, University of Lausanne, Lausanne, Switzerland, [2]Interdisciplinary Centre on Mountain Research, University of Lausanne, Lausanne, Switzerland, [3]Eawag, Swiss Federal Institute of Aquatic Science and Technology, Surface Waters, Research and Management, Dübendorf, Switzerland, [4]Institute of Earth Sciences, University of Lausanne, Lausanne, Switzerland

Key Points:

- The triggering of a whiting event in a large peri-alpine lake depends on distinct processes acting both in the lake and across its catchment
- During the event, initial calcite precipitation occurs in the river-lake mixing zone due to specific hydrological and geochemical conditions
- The spatial patterns of the whiting plume are constrained by lake hydrodynamics and coupled to distinct precipitation mechanisms in the lake

Supporting Information:

Supporting Information may be found in the online version of this article.

Correspondence to:

N. Escoffier,
nicolas.escoffier@unil.ch

Citation:

Escoffier, N., Perolo, P., Lambert, T., Rüegg, J., Odermatt, D., Adatte, T., et al. (2022). Whiting events in a large peri-alpine lake: Evidence of a catchment-scale process. *Journal of Geophysical Research: Biogeosciences*, *127*, e2022JG006823. https://doi.org/10.1029/2022JG006823

Received 25 JAN 2022
Accepted 29 MAR 2022

Author Contributions:

Conceptualization: Nicolas Escoffier, Marie-Elodie Perga
Data curation: Nicolas Escoffier
Formal analysis: Nicolas Escoffier, Daniel Odermatt, Thierry Adatte, Torsten Vennemann
Funding acquisition: Marie-Elodie Perga
Investigation: Nicolas Escoffier, Pascal Perolo, Thibault Lambert
Project Administration: Marie-Elodie Perga

Abstract Whiting events are transient phenomena commonly occurring in hardwater lakes and manifesting as a turquoise coloration of surface waters during massive calcium carbonate precipitation. While biological and physico-chemical drivers of carbonate precipitation are known, their relative contributions in controlling whiting events' timing and spatial extent remain poorly understood. Coupling spatially resolved data obtained for two sampling surveys using multiple analytical techniques and geochemical modeling, this study investigated the mechanisms underlying a whiting event during the early summer of 2019 in Lake Geneva. Satellite observations showed that the phenomenon started during a snowmelt period in the catchment at the Rhône River delta before spreading along the lake's northern shore and covering vast areas of its deeper basin. Authigenic calcite precipitated at the river mouth during mixing of warmer calcite super-saturated lake surface waters with colder snowmelt-diluted, sediment-rich river water containing detrital carbonates as potential nucleation sites. The development of the whiting event depended upon the thermal stratification of the water column and the existence of a physically stable metalimnion, within which a river interflow transported finer particles across the lake. During transport, the whiting plume enriched in authigenic carbonates by settling of coarser detrital particles and additional precipitation likely both on the fine-grained carbonate fraction and through biologically induced mechanisms in the superficial layers of the lake. This study provides novel mechanistic insights on the conditions controlling whiting events in lakes, highlighting a tight coupling of their dynamics with processes acting at the catchment scale.

Plain Language Summary Some lake waters can transiently and suddenly turn to a bright turquoise coloration, which results from the formation of fine particles of calcium carbonate during so-called whiting events. While the primary mechanism operating in whiting events (i.e., calcium carbonate precipitation) is known, current knowledge does not explain well the timing of these phenomena, nor their patchy spatial distribution in large lakes. Herein, we combined both large (from satellite data), medium-scale and small-scale observations, along with modeling, to investigate a whiting event in the largest lake of Western Europe, Lake Geneva. We show that this whiting event is a compound phenomenon whose timing is determined by a conjunction of specific thermal, biological, and geochemical conditions occurring both in the lake and in its main tributary, the Rhône River. The spatial extent of the whiting event is then driven by the lake water circulation, with a greater extension as the water column of the lake is more stratified. Our study gives supporting evidence to the tight coupling existing between lakes and their catchments and underscores an overlooked role of river-lake transition zones as important biogeochemical reactors.

1. Introduction

The global carbonate cycle plays a major role in the functioning of the Earth system and involves dissolution and precipitation reactions mediated by biogeochemical processes operating at distinct time scales (Ridgwell & Zeebe, 2005). Over geological time scales, carbonate reactions are considered ineffective in regulating atmospheric CO_2 as continental weathering of carbonates consuming CO_2 is offset by oceanic depositions that release CO_2 (Calmels et al., 2014). However, at shorter time scales, the carbonate cycle is intimately embedded within the carbon cycle, and its dynamics constrains major transformations across the organic and inorganic carbon reservoirs (Szramek & Walter, 2004). In inland waters, these controls also vary spatially, and the dynamics of carbonate cycling constrains different processes along the aquatic continuum. Carbonate weathering, for instance,

Writing – original draft: Nicolas Escoffier
Writing – review & editing: Nicolas Escoffier, Pascal Perolo, Thibault Lambert, Janine Rüegg, Daniel Odermatt, Thierry Adatte, Torsten Vennemann, Marie-Elodie Perga

may consume large amounts of atmospheric CO_2 (Liu et al., 2018), transferring it to the dissolved inorganic carbon (DIC) reservoir (Duvert et al., 2019). Reciprocally, in high alkalinity streams and lakes, CO_2 supersaturation and evasion may directly be attributed to the DIC supply from the watershed and related to carbonate buffering and precipitation reactions (Marcé et al., 2015; Stets et al., 2017).

Calcium carbonate (calcite) precipitation ($CaCO_{3(s)}$, Equation 1) is a prevalent process in hardwater lakes and reservoirs and represents a relevant term of the global lacustrine carbon budget (Khan et al., 2022).

$$Ca^{2+} + 2HCO_3^- \underset{Ks}{\leftrightarrow} CaCO_{3(s)} + CO_2 + H_2O \quad (1)$$

Calcite precipitation results from an oversaturation of water with respect to calcite, which can be due to an increase in temperature, owing to the retrograde solubility of calcite (Ks), and/or to a rise in pH related to CO_2 loss by turbulent degassing or bio-assimilation (Kelts & Hsü, 1978; Khan et al., 2021). Besides the required oversaturation, precipitation is conditioned by the presence of appropriate seeds in the water column that allow the activation energy for crystal nucleation to be decreased (Stabel, 1986). Calcite precipitation represents a sink of inorganic carbon in lakes through sediment storage (Khan et al., 2022). Because calcite may coprecipitate with important nutrients such as phosphate, the calcite sedimentation flux may also foster nutrient burial and have important implications for the trophic state and primary production of lacustrine systems (Heine et al., 2017).

Calcite precipitation can occur at low background levels over the warm summer season; however, massive short-term pulses may also manifest as so-called whiting events. Whiting events are transient phenomena corresponding to a milky blue coloration of surface waters that have been evidenced through satellite imagery in several hardwater lakes in Europe (e.g., Heine et al., 2017; Nouchi et al., 2019), across the Great Lakes area in North America (e.g., Binding et al., 2015; Strong & Eadie, 1978), as well as in marine coastal areas (e.g., Long et al., 2017; Morse et al., 2003; Shanableh et al., 2019). While the optical signature of whiting events has been related to fine-grained sedimentation of calcium carbonate (mainly calcite and aragonite in freshwater and marine systems, respectively) that enhances the reflectance of the water column (Peng & Effler, 2017), the underlying causes of their circumscribed occurrence in space and time have remained poorly understood.

Identifying the mechanisms of whiting events in aquatic systems has been a long-standing debate with distinct, sometimes conflicting, hypothesized, and evidenced drivers. In marine coastal zones, whiting events have mostly been explained by the precipitation of carbonates onto resuspended sediments (e.g., Bustos-Serrano et al., 2009; Dierssen et al., 2009; Morse et al., 2003), though some studies have evidenced a link with the presence of small phytoplankton cells or organic aggregates (Long et al., 2017; Sondi & Juračić, 2010). For lacustrine systems, a biologically induced inorganic origin of whiting events has more generally been proposed, relating calcite oversaturation and its precipitation to primary production and the presence of picoplankton, especially picocyanobacteria (e.g., Hodell et al., 1998; Peng & Effler, 2011; Thompson et al., 1997). Indeed, in the oligotrophic lakes where whiting events have commonly been observed, picoplankton constitutes a major component of the photosynthetic communities, and it has been shown to represent an effective site for heterogeneous precipitation (Dittrich & Obst, 2004). Preferential precipitation on picoplankton has been attributed to the local photosynthetically induced calcite supersaturation in the microenvironment of cells combined to a specific structure of membranes that acts as a relevant template for mineral nucleation (Dittrich et al., 2004; Thompson et al., 1997). Nevertheless, despite such mechanistic insights, substantial variability in the intensity, temporal and spatial extent of whiting events from 1 year to another has mainly remained unexplained (Binding et al., 2015). Moreover, some studies reported that calcite nucleation can occur on detrital mineral particles delivered to lacustrine systems by riverine allogenic inputs (Effler & Peng, 2012; Kelts & Hsü, 1978), complicating our understanding of the drivers of whiting events. Part of the uncertainty associated with the conditions driving whiting events may hence have originated from the complexity of the underlying physical and biological interactions (Hodell et al., 1998), as well as from the potential diversity of these relations across aquatic systems. Such a clear understanding may, furthermore, have been hampered by the difficulty to constrain heterogeneous processes over the vast areas that whiting events usually cover (Sondi & Juračić, 2010), as well as by the relatively limited number of in situ spatial studies that have examined these events (e.g., Long et al., 2017; Peng & Effler, 2011).

Lake Geneva is a particularly relevant example of a large lacustrine system with heterogeneous morphometric characteristics and distinct calcite precipitation features. Indeed, observations of calcite-coated grains and carbonate microspheres have been reported in the shallow western part of the lake and attributed to the photosynthetic

activity of biofilms in sediments or picoplankton in the water column, respectively (Jaquet et al., 2013; Plée et al., 2010). However, evidence of whiting events has only been reported for the deep eastern part of the lake, which receives its major hydrological input from the upper Rhône River catchment. Nouchi et al. (2019) provided an extensive description of such a whiting event in Lake Geneva during the summer of 2014. Using remote sensing techniques and hydrological modeling, Nouchi et al. (2019) demonstrated that the whiting event was initiated at the Rhône intrusion into the lake and that its spatial extent corresponded to the dispersion path of riverine particles across the lake. They hypothesized that calcite precipitation was actively triggered on the surfaces of fine river particles transported within the lake, an assumption that could not be validated due to the lack of direct in situ observations. However, other mechanisms may have contributed to the initiation of this phenomenon at the river mouth. Considering that the Rhône River not only supplies most of the water but is also the primary source of phosphorus to the lake (Perga et al., 2016), the triggering of calcite precipitation at the river inflow may have resulted from a biologically induced mechanism linked to stimulated phytoplankton communities. Besides, how much of the observed whiting was actually due to precipitation within the lake remained uncertain as detrital carbonates eroded from the upper Rhône catchment may also be transported by the river (Filippi et al., 1997; Stutenbecker et al., 2018).

Our purpose was to delineate the mechanisms supporting carbonate precipitation and sedimentation during whiting events in Lake Geneva by focusing on a specific event that occurred during 4 weeks of early summer 2019. Using remote sensing combined with in situ resolved sampling, we aimed explicitly at refining (a) the conditions underlying the triggering of such an event and the corresponding implication of processes occurring in the Rhône River catchment; (b) the origin of calcite particles (detrital or authigenic) during the event and the potential mechanisms supporting authigenic precipitation; and (c) the spatial dynamics of the whiting phenomenon in relation to hydrological mixing and transport across the lake.

2. Materials and Methods

2.1. Study Area

Lake Geneva (372 m above sea level) is the largest lake in Western Europe, with a surface area of 580 km^2 and a mean water residence time of about 11 years (Figure 1). Lake Geneva is divided into two basins. The Petit Lac and Grand Lac hold 4% and 96% of the total water volume and have a maximum depth of 70 and 309 m, respectively (CIPEL, 2015). Lake Geneva is an oligomictic lake; indeed, the Petit Lac overturns completely every winter, while for the Grand Lac, full mixing happens only during exceptionally cold winters, every 7 years on average (Gaudard et al., 2017).

Lake Geneva's watershed covers around 7,395 km^2. The Alpine Rhône River in the eastern part accounts for the main hydrological inputs (70%–80%), while the tributaries draining the Jura mountains to the north-west and the pre-Alps in the south contribute the rest. Direct water inputs by precipitation are minor (1%–7%; Halder et al., 2013). The Rhône River is also the primary supply of sediment to the lake, with the sediment composition reflecting the main lithologies of the catchment. The External massifs are characterized by granites and gneiss; the Penninic nappes contain siliceous and minor carbonate-bearing metasedimentary rocks and ophiolitic source rocks (metabasalts, -gabbros, and ultramafic rocks), while the Helvetic nappes are mainly composed of carbonates. The hydrological and water quality parameters of the Rhône River are continuously monitored by the Swiss Federal Office for the Environment (FOEN) at the Porte-du-Scex station, 5 km upstream from the lake (Figure 1). At this location, the sediment supply is, on average, composed of 57% inputs from the External massifs, 23% from the Penninic nappes, and 20% from the Helvetic nappes (Stutenbecker et al., 2018).

Lake Geneva is a hardwater lake with moderately alkaline waters (i.e., 1.5–2 meq L^{-1}) due to carbonate weathering in the catchment (Zobrist et al., 2018). Dissolved carbon is dominated by the inorganic pool (~99%), and pH is generally higher than 8.1 in the epilimnion during summer. Lake Geneva has returned to oligomesotrophic conditions after severe eutrophication in the 1970s (Perga et al., 2016).

2.2. Satellite Data

Daily wide-swath, medium-resolution (300 m) satellite images of Lake Geneva by Sentinel-3 A/B were downloaded from the Copernicus Open Access Hub (https://scihub.copernicus.eu/) using the Python package SenCast

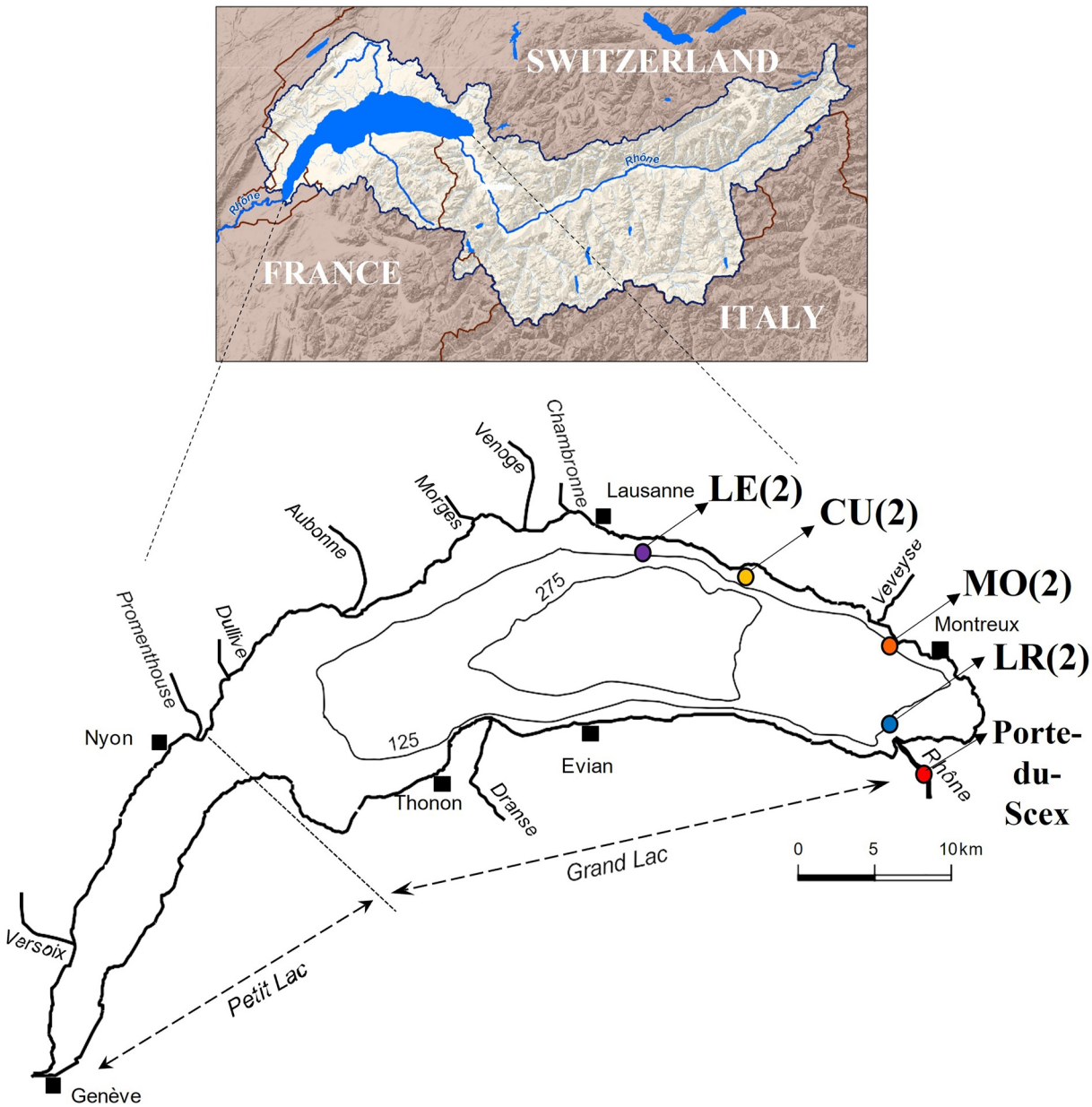

Figure 1. Lake Geneva watershed and location of the different stations sampled in the lake during the two surveys and in the Rhône River during the second survey.

(https://gitlab.com/eawag-rs/sencast). The data were atmospherically corrected, and normalized water-leaving reflectance (R_w) was calculated using the Polymer algorithm v4.13 (Steinmetz & Ramon, 2018), which was tried and tested for lake water quality retrieval in the Copernicus Global Land Service (Copernicus, 2020) and ESA's Climate Change Initiative (ESA, 2020). Polymer was configured to use the bio-optical model by Park and Ruddick (2005), and all pixels producing negative R_w at 665, 681, or 709 nm were removed from further analysis. According to suggestions by Heine et al. (2017), we calculated the triangle area as well as spectral integrals using OLCI bands at 490, 560, and 665 nm. Both are highly correlated with water-leaving reflectance at 560 nm, which is also the wavelength of maximum reflectance for all images acquired during the investigation period. Validation of Polymer products with R_w matchup measurements from an automated optical profiler in the years 2018–2020 showed that R_w at 560 nm is much more accurately retrieved than at other wavelengths; therefore, we henceforth refer to R_w at 560 nm as the indicator for calcite abundance. Sentinel-2 A/B imagery was processed

similarly using SenCast and Polymer but the CreoDIAS API (https://creodias.eu/) for data download. We used 10 m resolution true color composites for complementary illustrations.

2.3. Sampling Strategy

The sampling strategy was designed to compare the conditions before and during a whiting event in the lake and implemented according to the precedent observations by Nouchi et al. (2019) and the daily satellite images acquired by Sentinel-3 A/B. Lake Geneva was consequently sampled during two different campaigns: 12th to 14th of June 2019 and 27th to 28th of June 2019. Four sampling locations were pre-selected according to the main hydrological pathway of the Rhône River water dispersion in the Grand-Lac (Cimatoribus et al., 2019), and to cover a gradient of influence from its intrusion in the lake (Figure 1). Sampling points were located at a distance ranging between 750 m and 20 km from the river intrusion. Their notation, without or with the suffix 2 throughout the rest of the manuscript, refers to results obtained during the first or second sampling campaign, respectively.

At each site in the lake, water column profiles were sampled from a Zodiac boat using an EXO2 multiparameter probe equipped with EXO conductivity/temperature, pH, turbidity, and total algae (as Chlorophyll *a* (Chl*a*)) sensors (Yellow Spring Instruments Incorporated), all pre-calibrated in the laboratory. Profiles were processed directly on board to define four sampling depths per site corresponding to the subsurface (i.e., 0.5 m), the turbidity maximum (ranging between 7 and 15 m), the lower metalimnion (20–25 m), and near hypolimnetic conditions (i.e., at 60 m). For each depth, 10 L of water were collected using a Niskin bottle (KC-Denmark) and stored in pre-acid washed and pre-rinsed polyethylene containers before filtration in the laboratory on the same day. For partial pressure of CO_2 (pCO_2) measurements, three 60 ml pre-cleaned and pre-rinsed polyethylene syringes were used per depth on the boat to collect 30 ml of raw water without air bubbles. Moreover, due to EXO2 pH smart sensor malfunction during the first campaign, pH and specific conductance (at 25°C) values were also measured during the second campaign for each sampled depth immediately on board in the 10 L containers using a complementary multiparameter probe (Multi 3430, Set G, WTW) equipped with SenTix 940 and TetraCon 925 sensors pre-calibrated in the laboratory.

During the second campaign only, multiparameter measurements and water samples were also taken from the Rhône River at Porte-du-Scex. In addition, data on the main hydrological variables at the Porte-du-Scex monitoring station covering the period of both sampling campaigns were provided by the FOEN.

2.4. Analytical Procedures

2.4.1. Dissolved Species

For the determination of major ions, soluble reactive phosphorus (SRP), total alkalinity (TA), $\delta^{13}C$ of DIC ($\delta^{13}C$-DIC), and oxygen isotopic compositions, the collected raw water was filtered through 0.22 µm pore size polyethersulfone (PES) syringe filters (Minisart, Sartorius AG). Samples were then stored at 4°C in the dark in pre-rinsed pre-acid washed glass vials or sterile polypropylene tubes (Greiner Bio-One) until analyses within 2 weeks, while also avoiding any headspace for samples intended for isotopic analyses.

Major anion and cation concentrations, including nutrients as NH_4^+ and NO_3^-, were measured using ion chromatography (MetrOhm) with a detection limit of 0.1 mg L^{-1}. The SRP concentrations were determined by spectroscopy at 882 nm after reaction with ammonium molybdate and antimony potassium tartrate, and subsequent reduction by ascorbic acid, with a precision of 7%. The TA was determined by colorimetric titration using a SmartChem 200 analyzer (AMS Alliance). For TA, the methyl-orange titration to a final pH of 3.2 was used, achieving a precision of 2% on externally prepared standards. The oxygen isotopic compositions of water samples were measured with a Picarro L2140i (Picarro) using wavelength-scanned cavity ring-down spectroscopy (WS-CRDS). Sequence analyses included three standards calibrated against the international Vienna Standard Mean Ocean Water (VSMOW) from the International Atomic Energy Agency (IAEA), whose values were used to normalize sample results (Halder et al., 2013). Sample isotopic compositions are reported in common delta units (‰) relative to VSMOW. The standard deviation of all measured samples and standards was ±0.04‰ for $\delta^{18}O$. For $\delta^{13}C$-DIC analyses, a known volume of filtered water samples was injected in 12 mL Exetainer glass vials (Labco) containing ~300 µl of H_3PO_4 (85%) and having been previously flushed with He. All DIC species

were converted to CO_2 that was measured with a Gasbench II coupled to a Thermo Finnigan Delta Plus XL mass spectrometer (Spötl & Vennemann, 2003). Results were normalized against the in-house Carrara Marble II standard used during analyses and standard deviations of sample analytical replicates were always lower or equal to ±0.1‰ also measured for the standards. Results are expressed in the common delta (‰) units relative to the Vienna Pee Dee Belemnite (VPDB) international standard. pCO_2 values were determined in triplicates using the air-water syringes technique. 30 ml of atmospheric air was added to the syringes containing the 30 ml of water collected in the field and allowed to equilibrate after 5 min of vigorous shaking by hand. The equilibrated gas-phase pCO_2 was then measured with a non-dispersive infra-red (NDIR) analyzer (LI-COR, LI-830) and in situ pCO_2 was back-calculated with the CO2sys software (Pierrot et al., 2006) using water temperature in the syringe and at the depth of measurement, and taking into account the initial pCO_2 atmospheric value in the headspace measured from an independent dry syringe as well as in situ pH and TA values.

2.4.2. Particulate Fraction

For total suspended matter (TSM) measurements, a known volume of water (ranging between 1 and 2 L) was filtered in triplicates through pre-combusted (4 hr at 450°C) and pre-weighed 0.7 µm pore size glass fiber filters (GF/F, Whatman) that were stored at −20°C in the dark until analyses within 1 month. An additional volume of water (200–400 ml) was also filtered in triplicates through pre-weighed 0.2 µm pore size polycarbonate filters (Nuclepore, Whatman) and kept frozen until measurements were made with scanning electron microscopy coupled to energy dispersive X-ray spectroscopy (SEM-EDX).

The TSM concentrations were determined by weighing filters after drying at 40°C for 24 hr. For SEM-EDX analyses, filters were dried according to the same conditions and a carbon coating (ca. 15 nm) was applied on sub-samples mounted on aluminum stubs covered with double-sided conductive carbon tape. Imaging was performed with a Tescan Mira II LMU SEM using an acceleration voltage of 20 kV. Semi-quantitative X-ray chemical microanalyses were obtained using an EDX Penta-FET 3× detector (Oxford Instruments) at a working distance of 21 mm.

Whenever enough dry material was collected on TSM filters, complementary analyses were performed in order to characterize the composition of suspended sediments. Bulk-mineral compositions were determined by X-ray diffraction (XRD) analyses directly on TSM filters using an X-TRA Thermo-ARL Diffractometer. Samples were analyzed according to an angular range 2θ of 5°–65° with a step size of 0.02° and a continuous scan mode. Semi-quantitative estimates of mineralogical composition were based on sample XRD patterns by using external standards with a precision between 5% and 10% for phyllosilicates and 5% for other types of minerals. For $\delta^{13}C$ and $\delta^{18}O$ bulk carbonate analyses, a known quantity of dry material (ca. 1 mg) was cautiously retrieved from the TSM filters and transferred into 12 mL Exetainer glass vials that were then flushed with He. Carbonates were converted to CO_2 by reaction with concentrated H_3PO_4 and measured with a Gasbench II coupled to a Thermo Finnigan Delta Plus XL mass spectrometer (Spötl & Vennemann, 2003). Results were normalized against the in-house standard (Carrara Marble II) also measured during analyses. The maximum standard deviation obtained on measured samples and standards was 0.05‰ for $\delta^{13}C$ and 0.1‰ for $\delta^{18}O$. Results are expressed in the common delta (‰) units relative to the VPDB international standard. Sample carbonate contents, expressed as calcite, were also estimated with a precision of 1% from the CO_2 released during reaction.

2.5. Geochemical Modeling

The calculations of carbonate saturation and precipitation, and the modeling of river-lake waters mixing at the river intrusion were performed using the open-source chemical equilibrium software Visual MINTEQ version 3.1 (https://vminteq.lwr.kth.se/). Such calculations and mixing modeling could only be performed for the conditions of the second campaign, as pH sensor malfunctioning and the lack of river water sampling prevented these approaches for the first campaign.

2.5.1. Calcium Carbonate Saturation

The saturation index Ω for calcite was calculated from Ca^{2+} and CO_3^{2-} activities (i.e., $\{Ca^{2+}\}$ and $\{CO_3^{2-}\}$) and the temperature-corrected solubility constant K_{s0} according to the following formula:

$$\Omega = \frac{\left\{Ca^{2+}\right\}\left\{CO_3^{2-}\right\}}{K_{s0}} \quad (2)$$

Chemical activities were calculated using the Debye-Hückel approximation and the ionic strength was determined from the measured concentrations of major anions and cations. $\{Ca^{2+}\}$ was determined from the measured Ca^{2+} concentration, accounting for its possible complexation and the neutral species. $\{CO_3^{2-}\}$ was calculated from CO_3^{2-} concentration computed from measurements of TA and pH. All chemical equilibrium constants were adjusted to measured temperatures according to Plummer and Busenberg (1982). Considering the measured concentrations of Ca^{2+} and TA below 2 mM and 4 meq L^{-1}, respectively, bicarbonate and carbonate complexes of Ca^{2+} did not represent more than 5% of the total concentrations (Kelts & Hsü, 1978; Stumm & Morgan, 2012).

2.5.2. River—Lake Water Mixing

The titration/mixing section of Visual MINTEQ was used to simulate the mixing of the Rhône River with Lake Geneva surface waters at the river intrusion during the second campaign and the resulting conditions in terms of calcium carbonate saturation and precipitation.

Mixing conditions were calculated according to an increasing proportion of lake water (i.e., 100/0%, 90/10%, 75/25%, 50/50%, 25/75%, and 0/100% of river/lake proportions) and using the physico-chemical conditions measured in the river and below the lake surface (0.5 m depth) at the LR2 sampling point. The temperature and pH values were calculated for each condition assuming conservative mixing and used in the software to constrain chemical equilibria and speciation, as described in the previous section. Two versions of the model were run. In the first one, the calcite saturation index as well as the major ions and DIC concentrations were calculated. In the second version, the possible solid species option was used to simulate what would be the concentrations of calcite precipitating at equilibrium in solution at each step and the resulting major ions and DIC species concentrations. The modeling exercise also included other carbonate minerals such as dolomite (disordered and ordered forms); however, no precipitates were obtained in any model outputs. This result is in agreement with the fact that below a molar ratio of Mg:Ca < 2, as is the case in both river and lake waters, only calcite and low-Mg calcite should form (Stabel, 1986). Hence, corresponding results are not further referred to.

In a subsequent modeling step, the river water composition, equilibrated after mixing with 50% of lake surface water and calcite precipitation at a specific concentration derived from isotopic analyses, was further mixed with lake surface water to obtain the proportions estimated from the oxygen isotopic mass balance (described in the section hereafter) at 15, 25, and 60 m depth at LR2. This last step was performed to verify that the water composition recalculated at greater lake depths could be explained by dilution with the equilibrated surface river/lake water.

2.6. Calculations of Mixing Proportions

The presence of a river interflow in the lake and the corresponding proportions of Rhône and lake waters mixed at selected sampling points were quantified from the following isotope mass balance equation (Halder et al., 2013):

$$\delta^{18}O_R \cdot x_R + \delta^{18}O_L \cdot x_L = \delta^{18}O_M \quad (3)$$

with $\delta^{18}O_R$, $\delta^{18}O_{L,}$ and $\delta^{18}O_M$ corresponding to the isotopic composition of the Rhône River, the average isotopic composition of lake water measured at 60 m depth during both campaigns and the isotopic composition measured at selected sampling points, respectively, and x_R and x_L being the mole fraction of river and lake water, respectively.

Assuming that $x_R + x_L = 1$, the Rhône water fraction in the interflow was estimated according to:

$$x_R = \left(\delta^{18}O_M - \delta^{18}O_L\right) / \left(\delta^{18}O_R - \delta^{18}O_L\right) \quad (4)$$

The same mass balance approach was used to estimate the authigenic carbonate fraction in the bulk carbonates. Following the approach of Aucour et al. (1999), C-isotope and O-isotope mass balance calculations were performed. The average isotopic composition of carbonates in Mesozoic rocks (i.e., $\delta^{13}C$ of about 1‰, $\delta^{18}O$ of −5.5‰) was used for the detrital end-member, while the theoretical domain of authigenic precipitation at isotopic equilibrium was calculated from water temperatures and corresponding $\delta^{18}O$ and $\delta^{13}C$-DIC values measured between the surface and 25 m depth at the LR point for each campaign. The equilibrium fractionation factor (α) for oxygen isotope fractionation between water and calcite was calculated according to Kim and O'Neil (1997):

$$1000 \ln \alpha = 18.03 \,.\, 10^{3} \,.\, T^{-1} - 32.42 \quad (5)$$

while the equilibrium fractionation factor for carbon isotope fractionation between DIC (as HCO_3^-) and calcite was calculated according to Deines et al. (1974):

$$1000 \ln \alpha = 0.095 \,.\, 10^{6} \,.\, T^{-2} + 0.9 \quad (6)$$

with T as the water temperature in Kelvin.

3. Results

3.1. Whiting Event Dynamics in Lake Geneva and Hydrological Regime of the Rhône River

The whiting event in 2019 was observed for about 4 weeks from mid-June to mid-July with varying intensity and spatial extent within the lake (Figure 2). The first remote observation of increased R_w (560 nm) associated to a whiting's typical turquoise optical signature was acquired around the Rhône estuary on June 13, 2019 during the first sampling campaign. Cloudy weather prevented detailed observations during the successive days, until the same signature was imaged on June 17th and, particularly, June 19th when enhanced R_w was observed on a larger area. The optical signature of the event developed further across the lake during the consecutive weeks. Maximum R_w values were consistently measured at the river-lake mixing zone while lower and heterogeneous values were mostly observed along the northern lake shore. On certain dates, these spatial gradients were also characterized by gyre-like circulation patterns covering a large section of the Grand-Lac (e.g., on June 24th and 29th). Whiting reached its maximum intensity at the end of June, when the second campaign was realized, and in early July. It then progressively started to disappear and was barely visible by July 14th.

The whiting event coincided with a marked increase of the Rhône River discharge from 200 $m^3\ s^{-1}$ in early June to 700 $m^3\ s^{-1}$ in early July, and a maximum value of 850 $m^3\ s^{-1}$ measured on June 11th (Figure 3). The increasing discharge was accompanied by a rise of the river's suspended load and turbidity until early July, with several peaks coinciding with discharge peaks (e.g., on June 11th and July 2nd). Turbidity values then decreased during July as the whiting progressively disappeared from the lake. Such hydrological patterns were related to warming ambient air temperatures in the study area and a progressive decrease of the river's specific conductance (from 310 µS cm^{-1} in early June to 165 µS cm^{-1} in early July; see Figure S1 in Supporting Information S1), indicative of the onset of snowmelt in the Upper Alpine Rhône catchment.

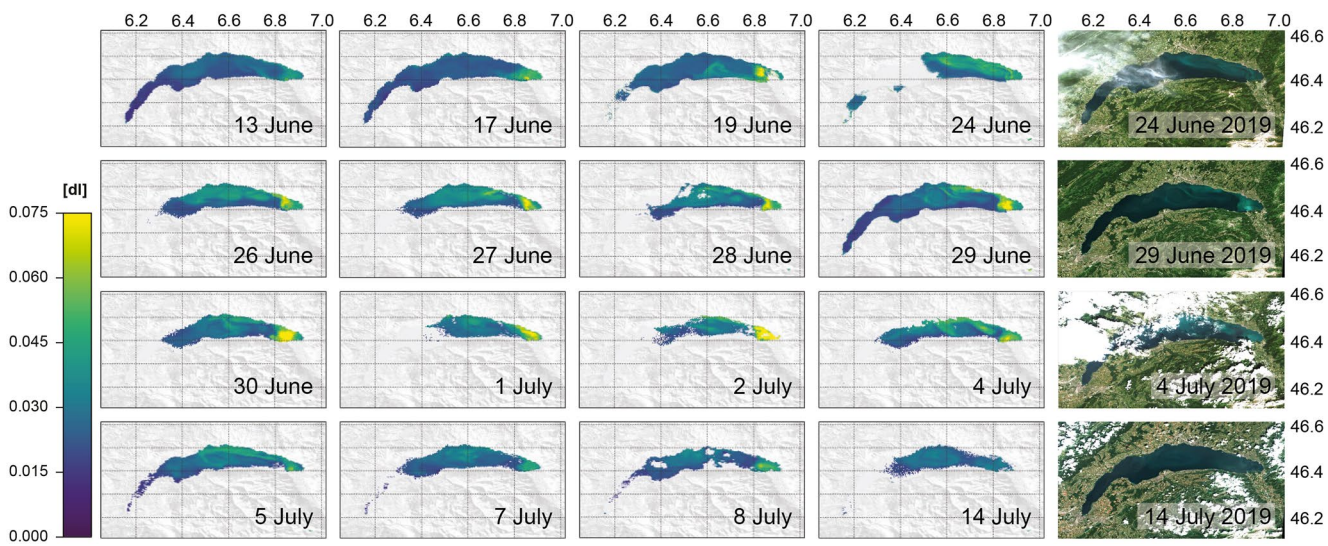

Figure 2. Spatial-temporal dynamics of the whiting event in Lake Geneva from June to July 2019, illustrated from Sentinel 3 A/B-derived daily water-leaving reflectance (R_w) at 560 nm (dimensionless [dl]) and from corresponding images of Sentinel-2 A/B at selected dates. The first sampling campaign was performed from 12th to 14th of June 2019 and the second campaign from 27th to 28th of June 2019. Coordinates *x* and *y* are given as longitudes and latitudes in decimal degrees, respectively.

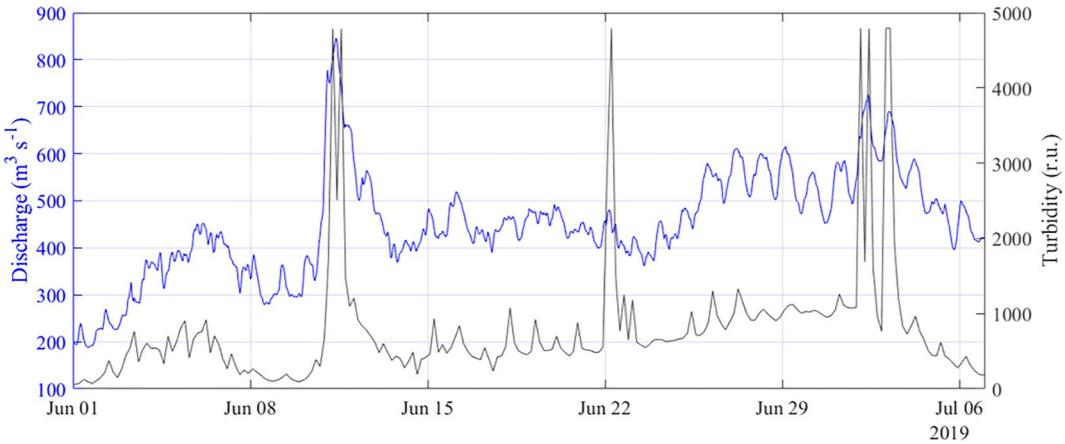

Figure 3. Time series of discharge (blue line) and turbidity (gray line) values recorded in the Rhône River at the Porte-du-Scex monitoring station (FOEN) over the period spanning the whiting event (i.e., June–July 2019).

3.2. Water-Column Biogeochemical Profiles

The profiles collected during both sampling campaigns evidenced that the development of the whiting event across the lake was associated with distinct spatial and temporal features in the water column. The beginning of the event coincided with the establishment of thermal stratification in the lake, with surface waters markedly increasing from 15°C to 25°C between campaigns (Figures 4a and 4e). In the river-lake mixing zone, at LR and

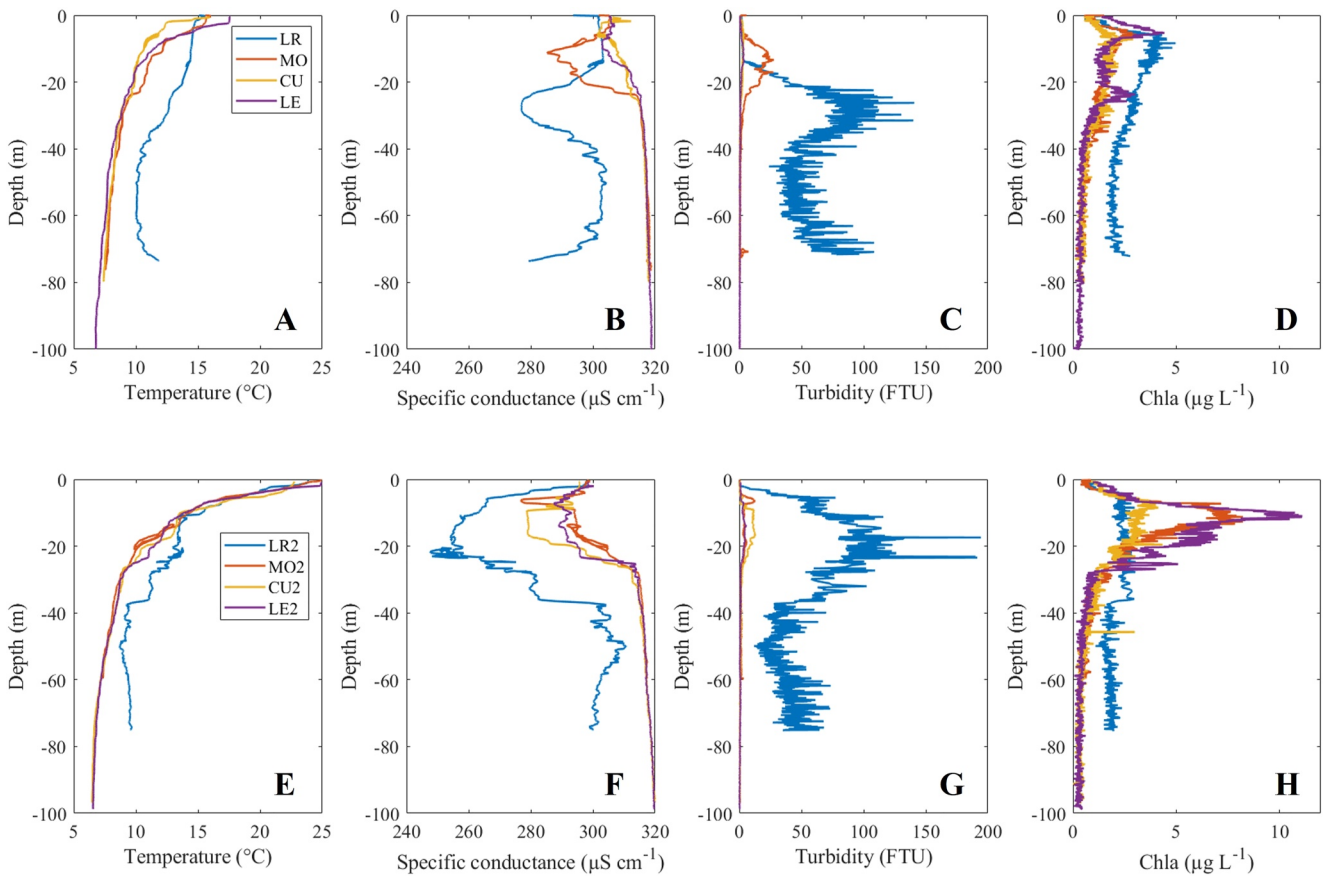

Figure 4. Water column profiles of temperature (a, e), specific conductance (b, f), turbidity (c, g) and Chl*a* (d, h) measured at the river mouth (LR-2) and at distal stations (MO-2, CU-2, and LE-2) before (i.e., first campaign June 12–14; (a–d) and during the whiting event (i.e., second campaign June 27–28; (e–h).

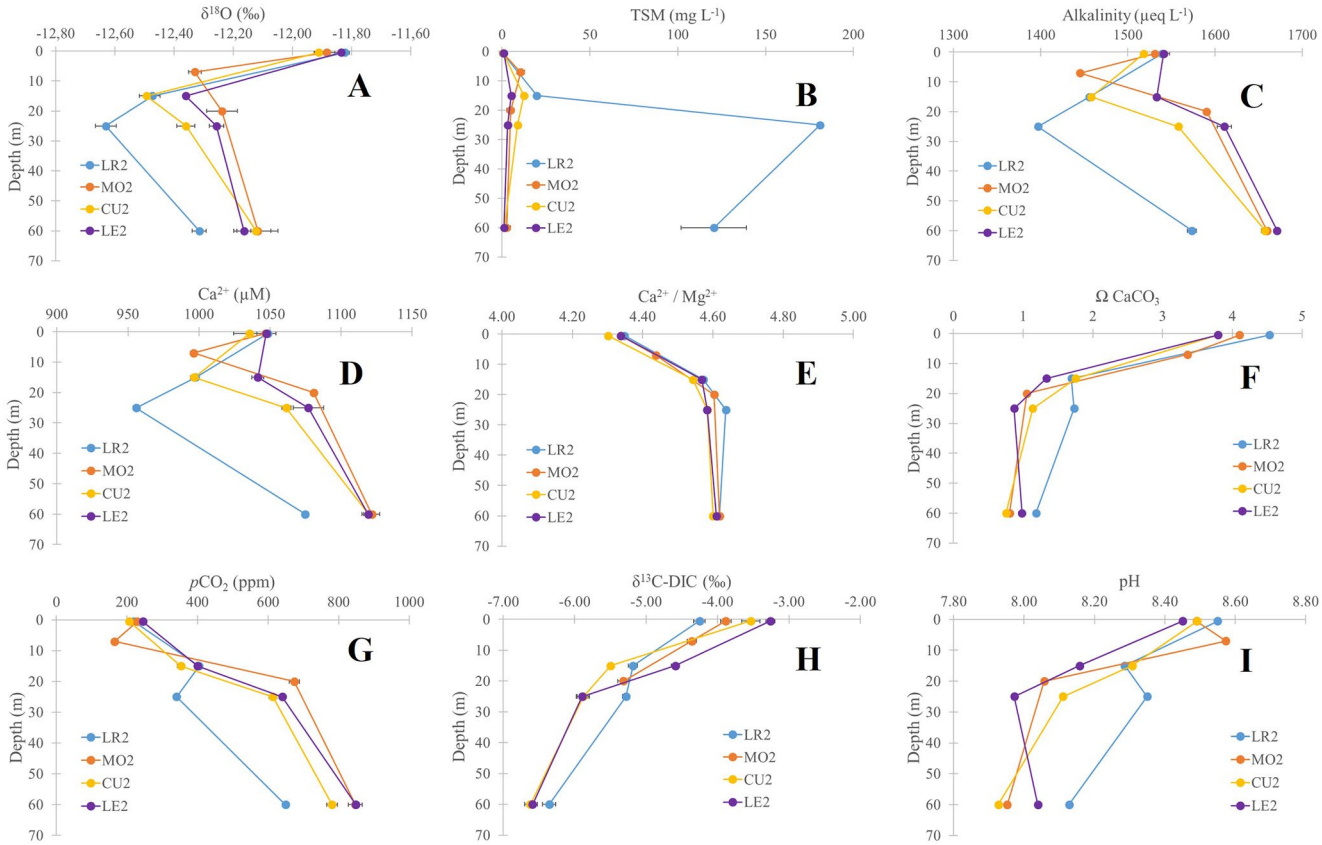

Figure 5. Profiles of O-isotope composition of water (a), Total Suspended Matter (b), Total Alkalinity (c), Ca^{2+}(d), Ca^{2+}/Mg^{2+}ratio (e), calcite saturation index Ω (f), partial pressure of CO_2 (g), $\delta^{13}C$ of dissolved inorganic carbon (h), and pH (i) measured at discrete depths of the four sampling sites of the second campaign during the peak of the whiting event.

LR2, the vertical temperature gradients were consistently lower than in other stations. Reciprocally, the profiles at these stations were characterized by stronger gradients of specific conductance and turbidity, with respective minimum and maximum values mirroring each other at depth (Figures 4b, 4c, 4f, and 4g). These gradients were more pronounced at LR2 during the second campaign and measured both at shallower depths and on a larger vertical layer. During the second campaign, the same patterns, though reduced, were also noted at MO2, CU2, and LE2 where maximum turbidity values were consistently observed in the metalimnion between ca 10 and 25 m depth. The development of the whiting event between campaigns was accompanied by an increase in Chl*a* concentrations at about 10 m depth in MO2 and LE2 (i.e., 8 and 11 µg L^{-1}, respectively), while values at other stations remained low and comparable to those measured during the first campaign (approx. 4 µg L^{-1} Figures 4d and 4h).

The analyses of discrete water samples from both campaigns evidenced that the depths of maximum turbidity and TSM concentrations consistently corresponded to layers having higher river water contributions (Figures 5a and 5b and Figures S2a and S2b in Supporting Information S1). The estimated fractions decreased with distance from the river mouth during both surveys; however, they showed that the propagation of river water as a turbid interflow was nearly two times more important for the second campaign (i.e., ranging from 10.2% to 25.5%). At this time of peak of the whiting conditions, the lower values of TA, Ca^{2+} and nutrient concentrations within the interflow (i.e., 15–25 m; Figures 5c and 5d and Figures S2d, S2f, and S2h in Supporting Information S1) could mostly be attributed to dilution by the lower snowmelt-related river concentrations (Table S1 in Supporting Information S1), as Ca^{2+}/Mg^{2+} ratios were consistent with deeper values (i.e., 60 m; Figure 5e) and coupled to relatively modest saturation levels (i.e., $\Omega \leq 1.8$, Figure 5f). Inversely, the concomitant lower Ca^{2+}/Mg^{2+} ratios and high level of calcite supersaturation in subsurface layers (ranging from 3.8 to 4.5) suggested that calcite precipitation occurred there, where enhanced primary production was also indicated by maximum pH, higher $\delta^{13}C$-DIC values (range, −3.3‰ to −4.3‰, Figure 5h) and substantially undersaturated pCO_2 values (i.e., <400

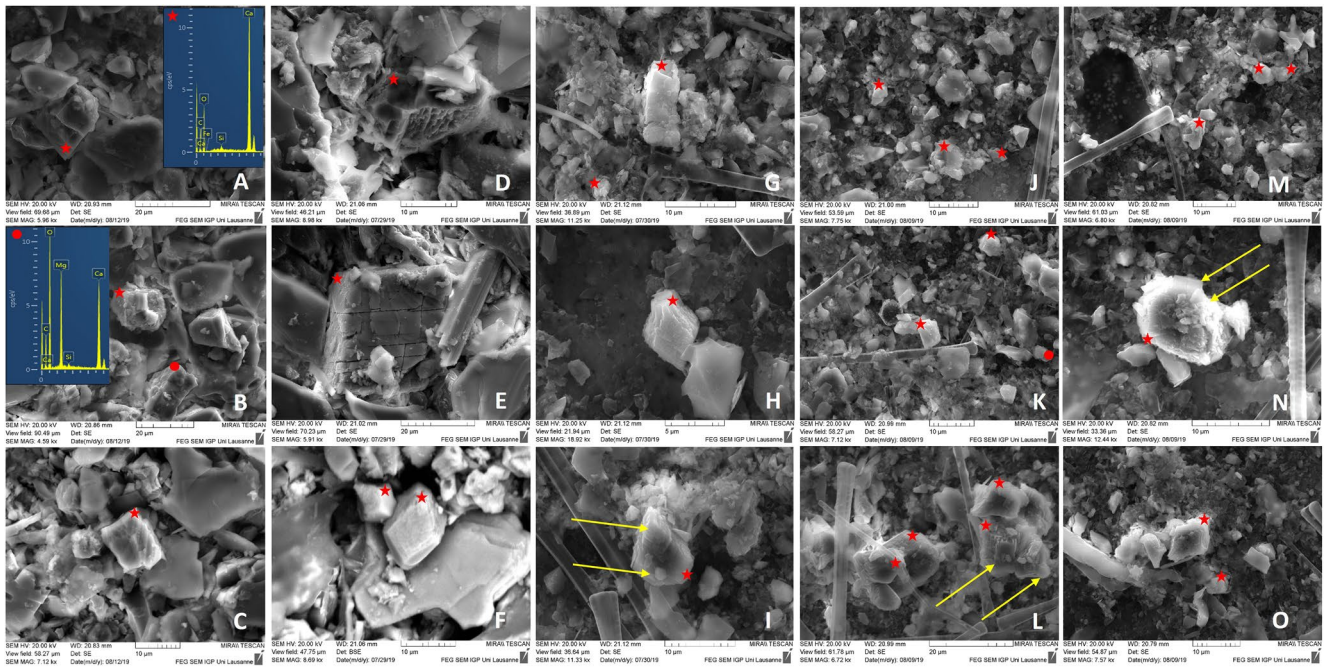

Figure 6. SEM images of suspended particles from the Rhône River (a–c) and from Lake Geneva at the river intrusion at LR2 (25 m, d–f) and within the river interflow at MO2 (7 m, g–i), CU2 (15 m, j–l) and LE2 (15 m, m–o) stations during the second campaign. Representative EDX scans for calcite (red star) and dolomite (red circle) particles are illustrated for the Rhône River (a, b). Yellow arrows indicate step-like and overgrowth patterns on crystals (i, l, n).

ppm atmospheric saturation, Figure 5g). Average sub-surface Ca^{2+}/Mg^{2+} ratios (i.e., 4.34) indicated a relative 5% loss of Ca^{2+} compared to deeper layers (i.e., averaging 4.58 between 15 and 60 m). Relating this depletion to the average Ca^{2+} concentration (i.e., about 1,100 µM) in subsurface for the first campaign or at depths not diluted by the river interflow for the second campaign (i.e., 60 m at MO2, CU2, and LE2), yielded a Ca^{2+} concentration decrease of 56 µM, equivalent to 5.6 mg L^{-1} precipitated as calcite.

3.3. Mineralogical and Structural Composition of Suspended Particles

The mineralogical composition of suspended sediments in the river and within the turbid layer across the lake was examined through XRD analyses before and during the peak of the whiting event. Such analyses showed a similar composition in the river and at its intrusion at 25 m depth in the lake at LR and LR2, with sediments made up of about 14%–16% of calcite, 3%–4% of dolomite, 25%–30% of phyllosilicates, 27%–28% of quartz, 3%–4% of K-feldspar, and 14%–17% of Na-plagioclase (Figure S3 in Supporting Information S1). Though slightly more variable, a comparable relative composition was also measured at 60 m depth during both campaigns. In terms of carbonate content, complementary analyses revealed that the proportion of carbonates within the turbid interflow decreased with distance from river intrusion during the first campaign (i.e., from 13% at LR to 7% at LE station), while it remained more stable across the lake during the second one (i.e., from 14% to 11%; Figure S3 in Supporting Information S1).

The relative consistency in carbonate content across stations of the second campaign was, however, associated with varying sizes and morphotypes of carbonate particles (Figure 6). In the Rhône River, the detrital calcite and dolomite particles occurred as eroded crystals with a range from 10 to 30 µm in size (Figures 6a–6c), and they occurred together with a wide granulometric size range of other sediment types (from several µm to several hundreds of µm). Similarly, large particles and eroded forms of calcite (~20 µm) were observed at the river mouth site at LR2 (Figure 6d), but they were accompanied by well-defined large rhombohedral (Figure 6e) and smaller diamond-shaped crystals (5–10 µm, Figure 6f). At the MO2, CU2, and LE2 sites, the average grain size was smaller (ranging between 5 and 10 µm, Figures 6g–6o) and carbonate morphotypes included amorphous crystals (e.g., Figures 6g and 6j) and diamond-shaped ones that were consistently identified. Some of these crystals were characterized by step-like growth features (e.g., Figure 6i) and overgrowths of secondary crystals (e.g., Figures 6l

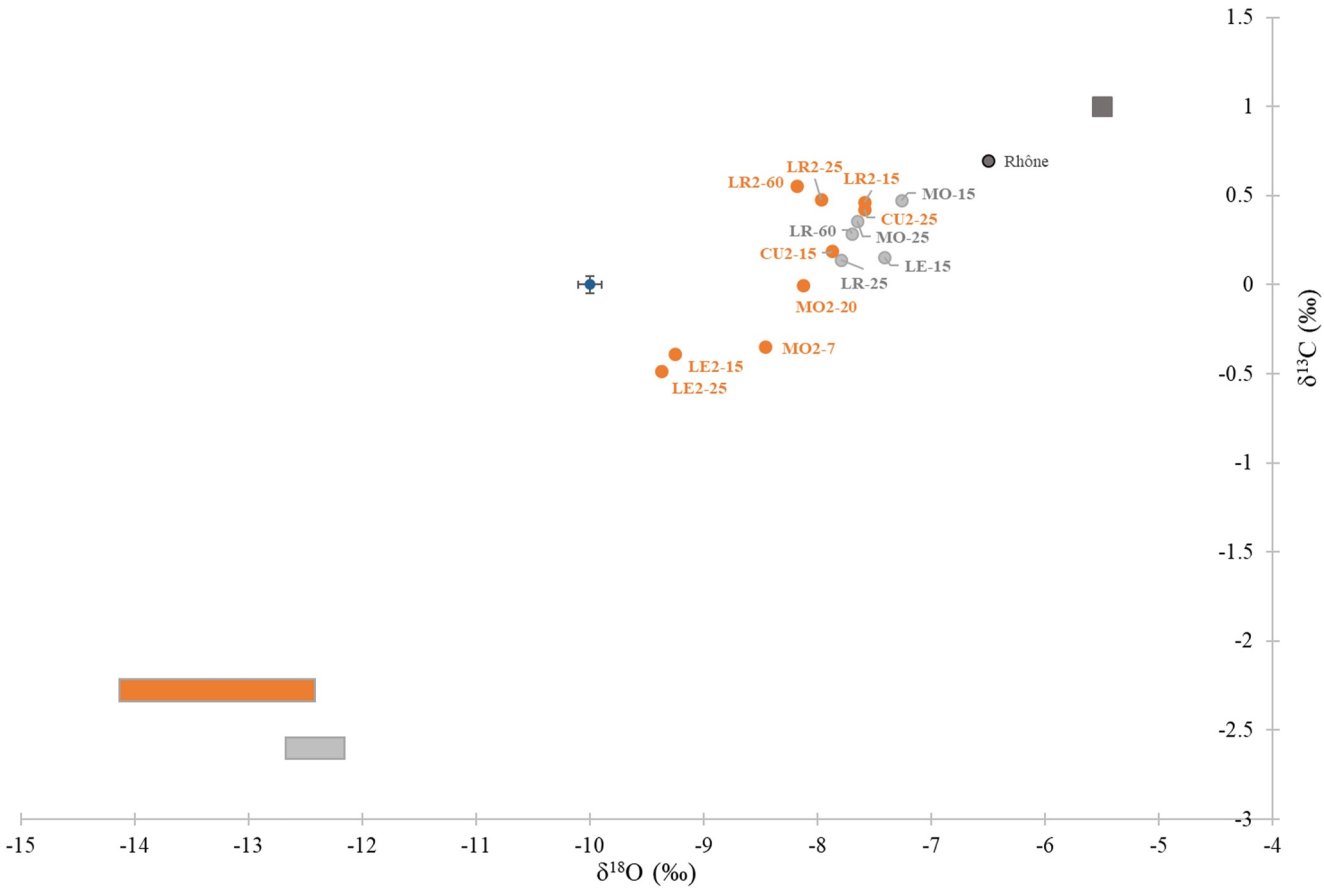

Figure 7. C-isotope and O-isotope compositions of carbonates in selected samples (indicated as site-depth) from the first (light gray circles) and second (orange circles) campaign. Compositions of the Rhône River carbonate fraction (dark gray circle) as well as values representing the detrital (dark gray square) and authigenic end-members for the first (light gray box) and second (orange box) campaign are also shown. Standard deviation (SD) is represented separately (blue circle) for clarity of the figure.

and 6n). Moreover, SEM analyses at the distal MO2, CU2, and LE2 sites, revealed the ubiquitous presence of large pennate diatoms (tentatively *Asterionella sp.*).

3.4. Isotopic Composition of Bulk Carbonates

All samples analyzed had isotopic compositions between the two end-members corresponding to the mean composition of detrital Mesozoic carbonates in the catchment and the theoretical values for authigenic carbonate precipitated at isotopic equilibrium calculated for the conditions of each campaign (Figure 7). Bulk isotopic compositions of the carbonate fraction in the Rhône (i.e., $\delta^{13}C = 0.7‰$, $\delta^{18}O = -6.5‰$) were also included for the second campaign, with slightly lower ^{13}C and ^{18}O content compared to the detrital end-member. For the first campaign, the suspended carbonates had relatively homogeneous isotopic compositions across stations (i.e., from $\delta^{13}C = 0.5‰$ and $\delta^{18}O = -7.3‰$ at 15 m at the MO station to $\delta^{13}C = 0.1‰$ and $\delta^{18}O = -7.8‰$ at 25 m at the LR station) and their further depletion in both ^{13}C and ^{18}O relative to detrital carbonates indicated an average of 30% of additional authigenic carbonates (Table 1). Additional carbonate precipitation was also confirmed during the peak of whiting conditions. However, the larger range of isotopic compositions (i.e., from $\delta^{13}C = 0.5‰$ and $\delta^{18}O = -7.6‰$ at 15 m at LR2 to $\delta^{13}C = -0.5‰$ and $\delta^{18}O = -9.4‰$ at 25 m at LE2), indicated an increasing authigenic content both with depth at LR2 (i.e., from 27.3% at 15 m to 34.9% at 60 m) and with distance from the river mouth (maximum value 50.4% at the LE2 station; Table 1).

In terms of absolute concentrations, these results indicated that total carbonate concentrations were similar at the river mouth for both campaigns (about 22 mg L^{-1} at 25 m; Table 1), including comparable maximum authigenic

Table 1
Total Concentration of Carbonates (as Calcite) Estimated From TSM Content and Based on Isotopic Analyses, and Corresponding Authigenic Fractions and Average Concentrations Derived From Isotope Mass Balance Calculations Using $\delta^{18}O$ Values

	Sample	TSM (mg L^{-1})	Total calcite (mg L^{-1})	Authigenic calcite (%)	Authigenic calcite (mg L^{-1})
#1st campaign	LR-25m	183.1 ± 14.5	23.0	33.5	7.71 ± 0.16
	LR-60m	139.3 ± 17.2	19.1	32.1	6.13 ± 0.13
	MO-15m	21.9 ± 0.5	3.3	25.7	0.84 ± 0.02
	MO-25m	8.3 ± 0.3	0.9	31.3	0.27 ± 0.01
	LE-15m	3.3 ± 0.2	0.3	27.9	0.07 ± 0.01
#2nd campaign	Rhône	614.3 ± 13.1	75.3	12.9	7.95 ± 2.48
	LR2-15m	19.8 ± 0.5	2.7	27.3	0.74 ± 0.11
	LR2-25m	181.1 ± 1	21.5	32.1	6.91 ± 0.95
	LR2-60m	120.6 ± 18.6	15.5	34.9	5.42 ± 0.74
	MO2-7m	10.5 ± 0.6	1.1	38.5	0.41 ± 0.06
	MO2-20m	4.8 ± 0.5	0.6	34.2	0.20 ± 0.03
	CU2-15m	12.4 ± 0.4	0.9	30.9	0.29 ± 0.04
	CU2-25m	8.8 ± 0.8	0.8	27.2	0.21 ± 0.03
	LE2-15m	5.2 ± 0.9	0.6	48.9	0.29 ± 0.04
	LE2-25m	3.2 ± 0.3	0.4	50.4	0.18 ± 0.02

concentrations (i.e., 7.71 ± 0.16 and 6.91 ± 0.95 mg L^{-1} at LR and LR2, respectively). During the first campaign, total and authigenic concentrations followed the same pattern as TSM values and decreased with increasing distance from the river mouth. In contrast, the slight decrease in total carbonate concentration from LR2 to LE2, for the second campaign, was compensated by the increase in authigenic content mentioned above. This resulted in relatively steadier authigenic concentrations in the turbid interflow at 15 m across the lake, with values ranging between 0.74 ± 0.11 and 0.29 ± 0.04 mg L^{-1} at LR2 and LE2, respectively. At this depth, particularly, the average concentration at LE2 was four times greater than its counterpart at LE during the first campaign (i.e., 0.07 ± 0.01 mg L^{-1}).

3.5. Mixing of River and Lake Waters

Simulations using river and lake water compositions from the second campaign were modeled to refine the conditions underlying calcite precipitation during initial mixing at the river mouth. The first modeling step showed that mixing river water with an increasing proportion of lake surface water at LR2 resulted in a linear increase in temperature along with nonlinear rising trends of the calcite saturation index and pH values (Figure 8). Calcite saturation levels were between the lower river value of 0.78 (Table S1 in Supporting Information S1) and upper lake one of 4.69. This would represent a maximum calcite concentration of 66.5 mg L^{-1} if precipitation was occurring at complete thermodynamic equilibrium and hence covers a range consistent with the concentrations measured in situ. More specifically, mixing of calcite undersaturated river water with 10% of lake surface water reached the calcite saturation equilibrium threshold value of 1, while further mixing at 50%–50% resulted in a saturation value of 2.5, and coincident temperature and pH values (i.e., 17°C and 8.53), interestingly, similar to conditions inferred down to 10 m depth at LR2 (Figures 4 and 5).

These equal mixing proportions were thus selected for the second modeling step, for which we used the corresponding water composition equilibrated after the precipitation of 5.6 mg L^{-1} of calcite, as derived from the measured Ca^{2+} depletion at the surface (Figure 5) and from authigenic concentration estimates at LR2 (Table 1). The resulting water was further mixed with lake surface water according to the proportions calculated at LR2 at 15, 25, and 60 m depth using a water O-isotope mass-balance approach. Assuming no further calcite precipitation, the modeling results indicated that the measured concentrations of major ions and DIC were reasonably well predicted by such a dilution mechanism (Table 2). At 15 and 25 m depth, the average quantification error

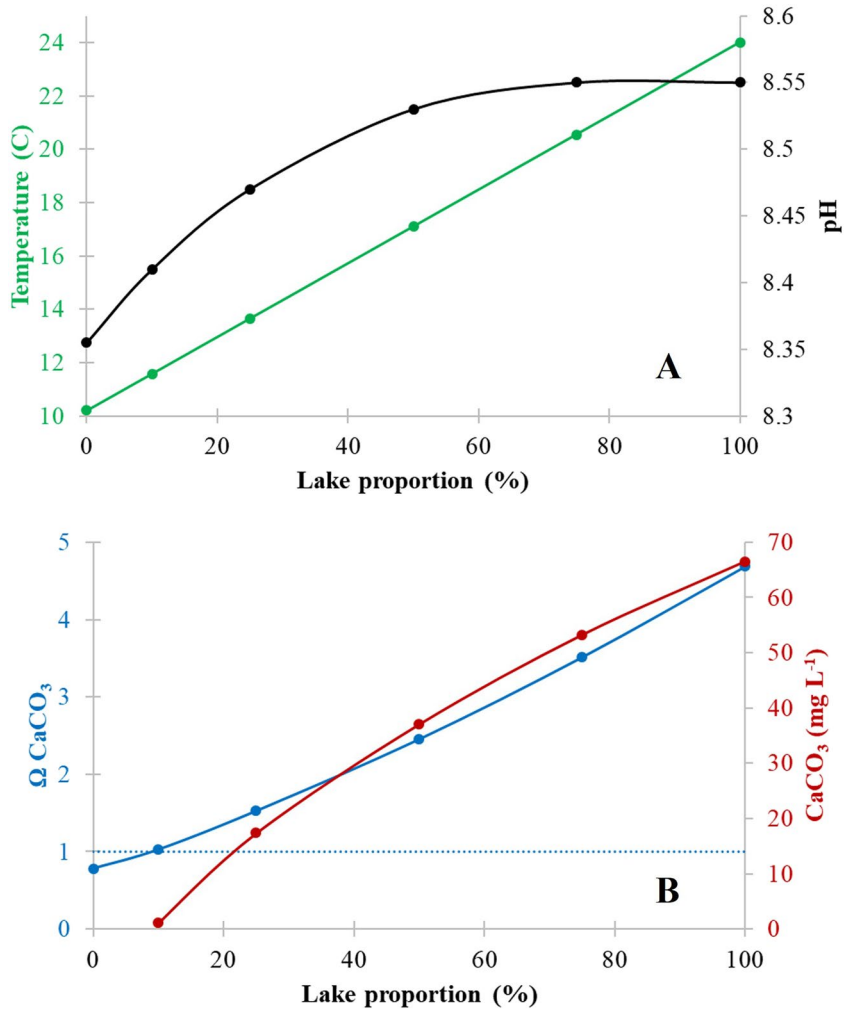

Figure 8. Simulation of the water temperature (green) and pH (black) resulting from mixing river water with increasing proportion of lake surface water at LR2 (a), and corresponding values of calcite saturation index Ω (blue) or concentrations (red), without or with precipitation enabled in the model, respectively (b). The dashed line in (b) represents the saturation equilibrium threshold value of 1.

on predicted concentrations reached −5.7 ± 4.1% and −5.9 ± 4.8%, respectively, while calcite saturation indices were slightly underestimated. A similar under-estimation of the saturation index was also obtained for the 60 m depth but coupled to a relatively higher average error on predicted concentrations (−9.7 ± 7.3%).

Table 2
Total Concentrations of Major Ions and DIC, pCO_2, and Calcite Saturation Index Values Measured at Several Depths at LR2 or Modeled From Dilution of the Equilibrated River/Lake Water (50/50%, Figure 8) After Calcite Precipitation, With Lake Surface Water, Using Mixing Proportions Derived From $\delta^{18}O$ Isotope-Balance Calculations

Sample	Ca^{2+} (µM)	Mg^{2+} (µM)	DIC (µM)	pCO_2 (ppm)	Ω $CaCO_3$
LR2-15m obs	997.6 ± 1.4	218.2 ± 0.6	1,430.3 ± 0.6	404 ± 3.3	1.69
model	937	216	1,360	360	1.59
LR2-25m obs	955.8 ± 2.3	206.2 ± 0.3	1,370.8 ± 2.9	340.5 ± 3.7	1.73
model	889	206	1,300	300	1.63
LR2-60m obs	1,074.7 ± 2.4	232.7 ± 0.4	1,573.4 ± 5.2	649.4 ± 6.2	1.19
model	988	227	1,430	521	1.05

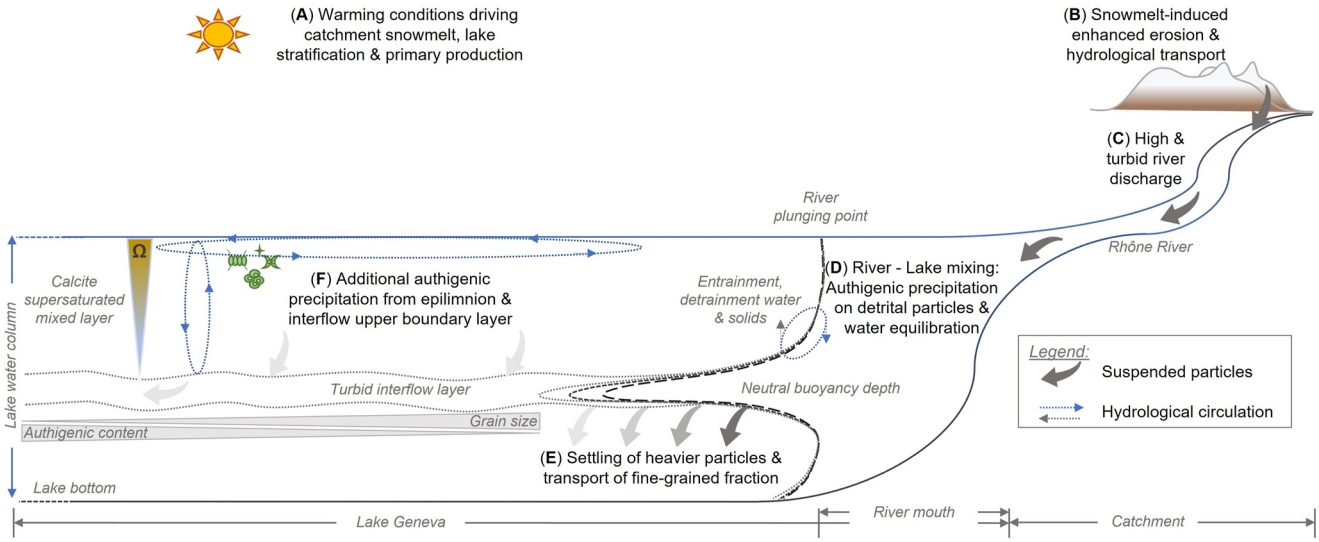

Figure 9. Conceptual model of the various processes contributing to the triggering and development of the whiting event in Lake Geneva. (a) Warming conditions across the catchment constrain the stratification of the lake, enhanced level of primary production in surface waters and snowmelt in alpine areas of the catchment. (b) The increase in hydrological connectivity and erosion due to snowmelt lead to (c) a high and turbid river discharge loading detrital suspended solids into the lake at the Rhône River mouth. (d) At this level, initial mixing between river and lake surface waters supports the authigenic precipitation of calcite on detrital particles, accompanied by entrainment and detrainment mechanisms of water and solids during the plunging and equilibration of the mixing water. Propagation of the resulting turbid whiting plume as an interflow at the depth of neutral buoyancy is characterized by a decrease in suspended particle size and increase in authigenic carbonate content due to (e) settling of the coarse-grained fraction and (f) additional authigenic precipitation from the upper interflow layer and biologically induced mechanisms in the epilimnion. Gray arrows refer to suspended solids while dashed lines represent hydrological circulation patterns.

4. Discussion

Calcite precipitation is a major biogeochemical process in hardwater lakes, and even though it represents an important component of the C budget, its dynamics at fine temporal and spatial scales remains poorly understood (Khan et al., 2021, 2022). This is especially true in the case of whiting events, which, due to their transient nature, represent understudied manifestations of calcite precipitation.

The results presented in this study help to refine the processes of formation for whiting events and, in the case of Lake Geneva, they corroborate previous elements that have linked such phenomena to the intrusion of the Rhône River (Nouchi et al., 2019). The 2019 event was first observed at the river mouth and its temporal dynamics, consistent with the 2014 event, followed an increase of river discharge and sediment load due to snowmelt in the alpine catchment. In situ data showed that the remote sensing reflectance signature of the event represented gradients of suspended particles within a turbid interflow corresponding to the dispersal of river water across the lake metalimnion. Accordingly, the spatial dynamics of the whiting event was consistent with the preferential deviation of the river interflow along the northern shore by Coriolis forces, followed by its propagation toward the Petit-Lac or alternative recirculation in the Grand-Lac within large wind-induced dominant gyres (Cimatoribus et al., 2019). Isotopic analyses supported a partly detrital allogenic origin of suspended carbonates within the whiting plume. Nevertheless, the observation of additional authigenic precipitation along specific hydrological and biogeochemical patterns provided further insights into the complex interplay of environmental conditions and precipitation processes underlying the dynamics of the whiting phenomenon across the lake. Figure 9 proposes a conceptual depiction of the corresponding mechanisms, which are further described in the following sections.

4.1. Conditions Supporting the Triggering of the Whiting Event at the River Mouth

The oversaturation of water with respect to calcite constitutes the first condition required for calcite precipitation and occurrence of the whiting event. In lacustrine systems, heterogeneous precipitation has been noted for saturation levels between 2 and 11 (e.g., Hodell et al., 1998; Kelts & Hsü, 1978; Stabel, 1986), and in hardwater peri-alpine lakes similar to Lake Geneva, a minimum value of 2.5 has more specifically been identified (e.g., Dittrich et al., 2004; Groleau et al., 2000). The saturation state of water is a function of Ca^{2+} and CO_3^{2-}

ionic product to calcite solubility, and it is ultimately constrained by temperature and pH. A noteworthy feature associated with the development of the whiting event between the two campaigns was the strong increase in lake surface temperature that characterized the onset of water column stratification (Figure 9a). The increasing stability was accompanied by the development of higher phytoplankton biomass (as Chl*a*) at certain stations and a resulting enhanced primary production in surface waters indicated by undersaturated pCO_2 values, higher δ^{13}C-DIC values, and increase in pH. Altogether these conditions contributed to increase the level of calcite saturation such that precipitation was thermodynamically viable from the surface of the lake down to about 10 m depth (Figure 5f). Maximum saturation levels were similar to conditions reported for whiting events in Lake Geneva (Nouchi et al., 2019) and other lacustrine or marine systems (e.g., Hodell et al., 1998; Long et al., 2017). However, while supersaturation is a required condition, it is not sufficient to induce precipitation if adequate nucleation grains are not present in the water column (Stabel, 1986).

Active calcite precipitation is supported by the authigenic carbonate content of the whiting plume and lower Ca^{2+}/Mg^{2+} ratios. However, the additional observations and measurements also suggest that these trends may result from distinct mechanisms in different parts of the lake. At the river mouth, which is a main focal area for the initial dynamics of the event, the high discharge-induced turbulence and levels of turbidity (Figures 9b and 9c), along with low nutrient inputs from the river were not conducive for phytoplankton development, as shown by the Chl*a* profiles (Figures 4d and 4h). Hence while local calcite supersaturation during the second campaign may have resulted from a legacy effect of primary production acting at longer timescales (Khan et al., 2021), the local precipitation of calcite may have been triggered by processes other than a nucleation on phytoplankton cells. The high river loading of suspended solids and its temporal coincidence with the whiting event may also have been important for authigenic carbonate precipitation, notably because of the high detrital carbonate content of the suspended solid fraction. Consistent with previous estimates at Porte-du-Scex by Stutenbecker et al. (2018), about 20% of detrital carbonates was present in the suspended sediment load (Figure S3 in Supporting Information S1) derived from erosion of the Helvetic nappes. Hence, a plausible explanation to the authigenic precipitation evidenced at LR and LR2 would be that nucleation proceeded on the surfaces of detrital carbonate grains loaded by the river. Such a mechanism of coating would indeed represent a thermodynamically efficient process to decrease the activation energy required for precipitation and, though not unequivocally identified on suspended sediments at LR2, it nonetheless is further supported by the relevant saturation levels maintained during initial mixing between river and lake waters (Figures 8, $\Omega \sim 2.5$ at 50%–50% mixing). A similar process has also been suggested in the case of marine whiting events and the presence of more soluble suspended carbonate-bearing phases may even enable precipitation at lower saturation levels (i.e., $\leq$1.8; Bustos-Serrano et al., 2009; Morse et al., 2003). Furthermore, such a triggering mechanism at the river mouth would also explain its temporal dynamics as a result of the enhanced provision of detrital grains to the super-saturated lake surface waters during the increased hydrological connectivity and sediment entrainment associated to snowmelt (Figures 9b–9d; Silva et al., 2019; Stutenbecker et al., 2018).

Beyond its triggering during initial surface mixing between river and lake waters, the subsequent development of the whiting event across the lake was nevertheless constrained by additional processes occurring at the river mouth (Figure 9d). In particular, the dynamics of calcite precipitation during plunging of the river is outlined by the vertical pattern of the bulk carbonate isotopic compositions. Calculated authigenic carbonate concentrations were similar at the LR and LR2 stations, however, decreasing δ^{18}O values of the carbonate fraction (Figure 7) suggested an increasing authigenic content with depth at LR2, while it remained constant at LR (Table 1). Such variation on the oxygen isotopic composition of inorganically precipitated calcite may result from different factors including the effects of temperature and pH as well as crystal growth rate (e.g., Watkins et al., 2014). In our study, the range of pH variation remained limited, suggesting that the isotopic pattern at LR2 more reasonably corresponded to the temperature-dependence of O-isotope fractionation. The temperature was indeed the parameter depicting the largest vertical gradients between the two sampling campaigns, as well as between the river and the lake (Figure 4 and Figure S1 in Supporting Information S1), and the observed pattern supports precipitation of calcite in warmer surface layers of the mixing zone (lower δ^{18}O values of the carbonate at higher temperatures), followed by its entrainment and accumulation at greater depths. Such assessment is consistent with the reported plunging of dense river water in Lake Geneva within a short distance from the shore (i.e., 100 $\pm$ 20 m; Sastre et al., 2010), involving an entrainment of particles and lake water at its upper boundary layer, while also potentially detraining some of the suspended solids toward the surface (Nouchi et al., 2019). During plunging, the river density changes as a result of continued mixing, and to some extent further carbonate precipitation, and it

finally assumes the form of an interflow at a depth range of about 10–25 m in this study, equivalent to its neutral buoyancy (Rueda et al., 2007). An important aspect is that the combined effects of precipitation in surface layers and cooling of the equilibrating water during plunging resulted in a decrease of pH and calcite saturation levels (Hodell et al., 1998; Morse et al., 2003), such that conditions at the depth of the newly formed interflow did apparently not allow further carbonate formation. The prevalence of a dilution pattern at the main sampled depth of the interflow (i.e., 15 m) seems supported by the results of the second modeling step at the river mouth as well as by the rather stable Ca^{2+}/Mg^{2+} ratios there, but also in distal locations. Collectively this suggests that the whiting plume mainly resulted from the dispersal of particles from the river mouth without additional precipitation, contradicting the former assumption by Nouchi et al. (2019). Nonetheless, the increasing authigenic carbonate content of the whiting plume with distance from the river estuary along depleted surface Ca^{2+}/Mg^{2+} ratios at other, more distal locations (i.e., MO2, CU2, and LE2) would tend to nuance this assessment and indicate that complementary precipitation processes contributed to shape the whiting dynamics across Lake Geneva.

4.2. Spatial Dynamics of the Whiting Event in Lake Geneva

Our results showed that while the conditions for calcite precipitation were already met at the river mouth during the first campaign, a major determinant for the development of the whiting event afterward across the lake can be linked to the higher physical stability of the water column and the establishment of a substantial interflow. During the corresponding hydrological transport, several mechanisms may have led to an increase in authigenic carbonate content along the whiting plume at distal locations (Figures 9e and 9f).

The transfer of the suspended load from the Rhône River into Lake Geneva, associated with the decrease in current velocity, results in a rapid settling of the coarser-grained sediment fraction (Dominik et al., 1993; Silva et al., 2019), such that the sole fine fraction may be transported over long distances within the interflow (Figure 9e; Dominik et al., 1983; Halder et al., 2013). Considering that initial precipitation at the river mouth has occurred as a coating on detrital carbonates, the loss of the coarse component from the plume involves that the fine transported particles should, owing to a higher surface-to-volume ratio, have a higher authigenic carbonate content. This is supported by the reduction in sediment granulometry from the river estuary and the observations of a fine grain size of carbonates morphotypes at distal stations (i.e., ∼5–10 μm, Figure 6). This process may therefore in part explain a higher authigenic fraction within the whiting plume as a result of particle size fractionation upon settling.

Other processes that may also have contributed to the observed trend should be related to the thickness of the interflow and its location within the water column, as well as to its residence time within the Grand-Lac (Figure 9f). While mostly sampled at 15 m, the turbid interflow was nevertheless detected on a wider depth layer, whose exact positioning at distal stations was likely constrained by the local stability of the water column and the combined effect of internal Kelvin waves (Cimatoribus et al., 2019; Halder et al., 2013). Our discrete sampling did not allow to fully resolve the profile of calcite saturation in the water column, however, coupled observations with turbidity profiles (Figures 4 and 5) indicate that the upper boundary layer of the interflow was still a thermodynamically relevant layer for calcite precipitation (i.e., $\Omega > 2.5$). This is also supported by the shallower sampling of the interflow at the MO2 station, where a higher saturation index was coupled to a lower Ca^{2+}/Mg^{2+} ratio (Figure 5). Moreover, at the MO2 as well as at the LE2 stations, the higher authigenic carbonate content of the whiting plume corresponded to a situation where the upper part of the interflow was encompassing the depth of maximum Chl*a* concentrations. Several processes may, therefore, be considered in order to explain the observed pattern of additional carbonate precipitation. First, local calcite supersaturation fostered by primary production in the upper part of the interflow, coupled to the increased residence time of fine sediments during transport in the lake, may have both allowed for further precipitation on the detrital carbonate particles. Then, biologically induced mechanisms of precipitation on phytoplankton cells in the metalimnion, in addition to epilimnion-derived precipitates, may too have contributed. The SEM images of carbonates from the whiting plume at distal locations support the occurrence of overgrowths and secondary crystals on the surface of fine particles (Figure 6). Conversely, the large diatoms did not appear as relevant sites for carbonate nucleation and we were not able to identify crystals resembling the forms induced by precipitation around picoplankton or organic particles described in other hardwater lakes (Dittrich et al., 2004; Peng & Effler, 2017). However, as overall lower Ca^{2+}/Mg^{2+} ratios were measured in superficial waters where enhanced primary production was prevalent, the implication of a biologically induced component of precipitation occurring in the upper layers and contributing to the authigenic carbonate content

of the whiting plume after settling cannot be excluded. As in other oligotrophic lakes subject to whiting events, picoplankton, and especially picocyanobacteria, have, indeed, been shown as major components of the phytoplankton biomasses developing in the mixed surface layer of the Grand-Lac during the stratified season (Parvathi et al., 2014; Personnic et al., 2009). Furthermore, a prominent role of these populations for the precipitation of carbonates has been demonstrated in the Petit-Lac (Jaquet et al., 2013; Martignier et al., 2017) as well as in other nearby peri-alpine lakes (Domaizon et al., 2013). Also, considering that the interflow may recirculate in dominant gyres for several weeks (Cimatoribus et al., 2019), during which vertical and lateral mixing events may homogenize the lake superficial layers (Figure 9f), discrete patterns of the whiting event at distal locations were likely to result from a combination of the aforementioned processes of carbonate precipitation acting in concert at the scale of this large lake. Such combined influence is precisely reflected in the gradient of allochthonous to autochthonous carbonate sediment facies documented at the bottom northern part of the Grand-Lac (Kremer et al., 2015), and, thereby, outlines the relevant contribution of whiting events to the overall carbonate sedimentation in Lake Geneva.

4.3. Whiting Events in Lacustrine Systems

The present study underlines that whiting events in Lake Geneva may result from a complex conjunction of environmental conditions and processes, whose concomitance is a likely main driver of the phenomenon's ephemerality. By combining macroscale to microscale pattern analyses, our findings provide further mechanistic insights into the determinism of whiting events in lakes, showing that they are not necessarily only triggered by endogenic processes. Indeed, while our results partly support the commonly accepted biological origin of these phenomena (e.g., Hodell et al., 1998; Strong & Eadie, 1978; Thompson et al., 1997), they also show that, in Lake Geneva, they can be constrained by the substantial remobilization of sediment across the catchment and corresponding riverine detrital inputs occurring during snowmelt. As such, our observations emphasize a potentially overlooked component of the phenology of these events in lakes, which shares a remarkable similarity with marine occurrences triggered by the resuspension of carbonate sediments (e.g., Bustos-Serrano et al., 2009; Morse et al., 2003). While this study may contribute to refining our current vision on the mechanisms underlying the formation of whiting events, the present results, along with their uncertainties, may also help clarify these phenomena in other lacustrine systems.

As elusive manifestations, whiting events have often been studied remotely, enabling large scale and eventually interannual observations but preventing a direct examination of the processes involved (e.g., Binding et al., 2015; Heine et al., 2017). Inversely, few studies have investigated the spatial dynamics of whiting events in situ (e.g., Hodell et al., 1998; Peng & Effler, 2011), and some confounding observations may have derived from the heterogeneity of conditions characterizing these phenomena over large areas (Sondi & Juračić, 2010). The presents results underline that a detailed combination of observational and analytical methods is required to describe the physical and biogeochemical interactions constraining the occurrences of whiting events. Moreover, as these events represent a short-term optical manifestation of calcite precipitation induced by the fine grain size of particles (Thompson et al., 1997), particular attention should be devoted to the nature and origin of the seeds supporting crystal nucleation. Indeed, while the conditions for calcite supersaturation may generally be related to the dynamics of primary production, its precipitation during whiting events may, on the other hand, occur on a variety of nuclei consistent with the optical phenomenon. The very few studies to characterize calcite "whiting" particles in different lakes indicated a mostly organic, and to a lesser extent mineral, origin of nuclei but associated to substantial unexplained variability in size and shape (Peng & Effler, 2011, 2017). Our results suggest a potential larger diversity of nuclei involved during whiting events whose origin may be considered in the perspective of the allochthonous inputs that lakes receive from their catchments.

Further investigations would hence be required in order to precise such considerations and assess the diversity of conditions that may support the occurrence of whiting events in lacustrine systems. While such evaluation should contribute to verifying the general relevance of our results, the large prevalence of lakes within carbonate-rich catchments (Marcé et al., 2015) would nevertheless suggest that the identified patterns may hold true in other freshwater systems. Considering that calcite precipitation represents a major inorganic carbon sink in inland waters (Khan et al., 2022) and that whiting events may materialize catalyzed periods of carbon transformations across catchments, a refined perspective on the conditions triggering these phenomena would, thereby, appear essential to accurately constrain lacustrine carbon budgets. Such assessment would, moreover, seem even more

relevant in the context of global change, especially in peri-alpine areas, as the combined effects of increasing temperatures, weathering rates, and altered hydrological regimes are likely to impact the complex balance of mechanisms and processes underlying these events.

Conflict of Interest

The authors declare no conflicts of interest relevant to this study.

Data Availability Statement

The physical and chemical data of the sampling campaigns are available on Zenodo (https://doi.org/10.5281/zenodo.6421494; Escoffier, 2022). The hydrological data of the Rhône River are available upon request from the Swiss Federal Office for the Environment (https://www.bafu.admin.ch/bafu/fr/home/themes/eaux/etat/donnees/obtenir-des-donnees-mesurees-sur-le-theme-de-l-eau.html). The satellite images are available from the Copernicus Open Access Hub (https://scihub.copernicus.eu/).

Acknowledgments
This study was funded by the Fonds National Suisse (FNS, CARGOGEN project 200021_175530). Water quality data for the Rhône River were kindly provided by the FOEN. The authors thank Laetitia Monbaron, Micaela Faria, Aurélien Ballu, Pierre Vonlanthen, and Jasmin Kesselring for assistance and Didier Jézéquel for his comments on the manuscript. The authors thank Vincent Nouchi and Rolf Scheuner for the implementation of Sencast and the EPFL Limnology Center for funding the project W-DOC. The authors also thank three anonymous reviewers for their helpful comments. Open access funding provided by Universite de Lausanne.

References

Aucour, A. M., Sheppard, S. M. F., Guyomar, O., & Wattelet, J. (1999). Use of 13C to trace origin and cycling of inorganic carbon in the Rhone river system. *Chemical Geology*, *159*(1–4), 87–105. https://doi.org/10.1016/S0009-2541(99)00035-2

Binding, C. E., Greenberg, T. A., Watson, S. B., Rastin, S., & Gould, J. (2015). Long term water clarity changes in North America's Great Lakes from multi-sensor satellite observations. *Limnology & Oceanography*, *60*(6), 1976–1995. https://doi.org/10.1002/lno.10146

Bustos-Serrano, H., Morse, J. W., & Millero, F. J. (2009). The formation of whitings on the Little Bahama bank. *Marine Chemistry*, *113*(1–2), 1–8. https://doi.org/10.1016/j.marchem.2008.10.006

Calmels, D., Gaillardet, J., & François, L. (2014). Sensitivity of carbonate weathering to soil CO2 production by biological activity along a temperate climate transect. *Chemical Geology*, *390*, 74–86. https://doi.org/10.1016/j.chemgeo.2014.10.010

Cimatoribus, A. A., Lemmin, U., & Barry, D. A. (2019). Tracking Lagrangian transport in Lake Geneva: A 3D numerical modeling investigation. *Limnology & Oceanography*, *64*(3), 1252–1269. https://doi.org/10.1002/lno.11111

CIPEL. (2015). Fiche signalétique du léman et de son bassin versant. *Rapport CIPEL Campagne 2014*.

Copernicus. (2020). *Copernicus global land operations "cryosphere and water" "CGLOPS-2"—Algorithm theoretical basis document lake waters 300m and 1km products versions 1.3.0-1.4.0 Issue I1.12*.

Deines, P., Langmuir, D., & Harmon, R. S. (1974). Stable carbon isotope ratios and the existence of a gas phase in the evolution of carbonate ground waters. *Geochimica et Cosmochimica Acta*, *38*(7), 1147–1164. https://doi.org/10.1016/0016-7037(74)90010-6

Dierssen, H. M., Zimmerman, R. C., & Burdige, D. J. (2009). Optics and remote sensing of Bahamian carbonate sediment whitings and potential relationship to wind-driven Langmuir circulation. *Biogeosciences*, *6*(3), 487–500. https://doi.org/10.5194/bg-6-487-2009

Dittrich, M., Kurz, P., & Wehrli, B. (2004). The role of autotrophic picocyanobacteria in calcite precipitation in an oligotrophic lake. *Geomicrobiology Journal*, *21*(1), 45–53. https://doi.org/10.1080/01490450490253455

Dittrich, M., & Obst, M. (2004). Are picoplankton responsible for calcite precipitation in lakes? *Ambio*, *33*(8), 559–564. https://doi.org/10.1579/0044-7447-33.8.559

Domaizon, I., Savichtcheva, O., Debroas, D., Arnaud, F., Villar, C., Pignol, C., et al. (2013). DNA from lake sediments reveals the long-term dynamics and diversity of *Synechococcus* assemblages. *Biogeosciences*, *10*(6), 3817–3838. https://doi.org/10.5194/bg-10-3817-2013

Dominik, J., Burrus, D., & Vernet, J. P. (1983). A preliminary investigation of the Rhone River plume in eastern Lake Geneva. *Journal of Sedimentary Petrology*, *53*(1), 159–163. https://doi.org/10.1306/212F817A-2B24-11D7-8648000102C1865D

Dominik, J., Dulinski, M., Daniel, S., Hofmann, A., Favarger, P.-Y., & Vernet, J.-P. (1993). Transfert de matière et de radio-isotopes entre l'eau et les sédiments dans le Léman. *Rapport CIPEL Campagne 1992*.

Duvert, C., Bossa, M., Tyler, K. J., Wynn, J. G., Munksgaard, N. C., Bird, M. I., et al. (2019). Groundwater-derived DIC and carbonate buffering enhance fluvial CO_2 evasion in two Australian tropical rivers. *Journal of Geophysical Research: Biogeosciences*, *124*(2), 312–327. https://doi.org/10.1029/2018JG004912

Effler, S. W., & Peng, F. (2012). Light-scattering components and Secchi depth implications in Onondaga Lake, New York, USA. *Fundamental and Applied Limnology*, *179*(4), 251–265. https://doi.org/10.1127/1863-9135/2012/0177

ESA. (2020). *D2.2: Algorithm theoretical basis document*.

Escoffier, N. (2022). Sampling campaign data – Lake Geneva [Dataset]. *Zenodo*. https://doi.org/10.5281/zenodo.6421494

Filippi, M. L., Moscariello, A., & Hunziker, J. (1997). Stable isotopes in Lake Geneva carbonate sediments and molluscs: Review and new data. *Eclogae Geologicae Helvetiae*, *90*(2), 199–210. https://doi.org/10.5169/seals-168154

Gaudard, A., Schwefel, R., Räman Vinnä, L., Schmid, M., Wuëst, A., & Bouffard, D. (2017). Optimizing the parameterization of deep mixing and internal seiches in one-dimensional hydrodynamic models: A case study with Simstrat v1.3. *Geoscientific Model Development*, *10*(9), 3411–3423. https://doi.org/10.5194/gmd-10-3411-2017

Groleau, A., Sarazin, G., Vinçon-Leite, B., Tassin, B., & Quiblier-Llobéras, C. (2000). Tracing calcite precipitation with specific conductance in a hard water alpine lake (Lake Bourget). *Water Research*, *34*(17), 4151–4160. https://doi.org/10.1016/S0043-1354(00)00191-3

Halder, J., Decrouy, L., & Vennemann, T. W. (2013). Mixing of Rhône River water in Lake Geneva (Switzerland-France) inferred from stable hydrogen and oxygen isotope profiles. *Journal of Hydrology*, *477*, 152–164. https://doi.org/10.1016/j.jhydrol.2012.11.026

Heine, I., Brauer, A., Heim, B., Itzerott, S., Kasprzak, P., Kienel, U., & Kleinschmit, B. (2017). Monitoring of calcite precipitation in hardwater lakes with multi-spectral remote sensing archives. *Water*, *9*(1), 15. https://doi.org/10.3390/w9010015

Hodell, D. A., Schelske, C. L., Fahnenstiel, G. L., & Robbins, L. L. (1998). Biologically induced calcite and its isotopic composition in Lake Ontario. *Limnology & Oceanography*, *43*(2), 187–199. https://doi.org/10.4319/lo.1998.43.2.0187

Jaquet, J. M., Nirel, P., & Martignier, A. (2013). Preliminary investigations on picoplankton-related precipitation of alkaline-Earth metal carbonates in meso-oligotrophic lake Geneva (Switzerland). *Journal of Limnology*, *72*(3), 592–605. https://doi.org/10.4081/jlimnol.2013.e50

Kelts, K., & Hsü, K. J. (1978). Freshwater carbonate sedimentation. In *Lakes* (pp. 295–323). New York: Springer. https://doi.org/10.1007/978-1-4757-1152-3_9

Khan, H., Laas, A., Marcé, R., Sepp, M., & Obrador, B. (2021). Eutrophication and geochemistry drive pelagic calcite precipitation in lakes. *Water*, *13*(5), 597. https://doi.org/10.3390/w13050597

Khan, H., Marcé, R., Laas, A., & Obrador, B. (2022). The relevance of pelagic calcification in the global carbon budget of lakes and reservoirs. *Limnética*, *41*(1), 17–25. https://doi.org/10.23818/limn.41.02

Kim, S. T., & O'Neil, J. R. (1997). Equilibrium and nonequilibrium oxygen isotope effects in synthetic carbonates. *Geochimica et Cosmochimica Acta*, *61*(16), 3461–3475. https://doi.org/10.1016/S0016-7037(97)00169-5

Kremer, K., Corella, J. P., Adatte, T., Garnier, E., Zenhäusern, G., & Girardclos, S. (2015). Origin of turbidites in deep Lake Geneva (France–Switzerland) in the last 1500 years. *Journal of Sedimentary Research*, *85*(12), 1455–1465. https://doi.org/10.2110/jsr.2015.92

Liu, Z., Macpherson, G. L., Groves, C., Martin, J. B., Yuan, D., & Zeng, S. (2018). Large and active CO2 uptake by coupled carbonate weathering. *Earth-Science Reviews*, *182*, 42–49. https://doi.org/10.1016/j.earscirev.2018.05.007

Long, J. S., Hu, C., Robbins, L. L., Byrne, R. H., Paul, J. H., & Wolny, J. L. (2017). Optical and biochemical properties of a southwest Florida whiting event. *Estuarine, Coastal and Shelf Science*, *196*, 258–268. https://doi.org/10.1016/j.ecss.2017.07.017

Marcé, R., Obrador, B., Morguí, J. A., Lluís Riera, J., López, P., & Armengol, J. (2015). Carbonate weathering as a driver of CO2 supersaturation in lakes. *Nature Geoscience*, *8*(2), 107–111. https://doi.org/10.1038/ngeo2341

Martignier, A., Pacton, M., Filella, M., Jaquet, J. M., Barja, F., Pollok, K., et al. (2017). Intracellular amorphous carbonates uncover a new biomineralization process in eukaryotes. *Geobiology*, *15*(2), 240–253. https://doi.org/10.1111/gbi.12213

Morse, J. W., Gledhill, D. K., & Millero, F. J. (2003). CaCO3 precipitation kinetics in waters from the Great Bahama Bank: Implications for the relationship between Bank hydrochemistry and whitings. *Geochimica et Cosmochimica Acta*, *67*(15), 2819–2826. https://doi.org/10.1016/S0016-7037(03)00103-0

Nouchi, V., Kutser, T., Wüest, A., Müller, B., Odermatt, D., Baracchini, T., & Bouffard, D. (2019). Resolving biogeochemical processes in lakes using remote sensing. *Aquatic Sciences*, *81*(27). https://doi.org/10.1007/s00027-019-0626-3

Park, Y. J., & Ruddick, K. (2005). Model of remote-sensing reflectance including bidirectional effects for case 1 and case 2 waters. *Applied Optics*, *44*(7), 1236–1249. https://doi.org/10.1364/AO.44.001236

Parvathi, A., Zhong, X., Ram, A. S. P., & Jacquet, S. (2014). Dynamics of auto- and heterotrophic picoplankton and associated viruses in Lake Geneva. *Hydrology and Earth System Sciences*, *18*(3), 1073–1087. https://doi.org/10.5194/hess-18-1073-2014

Peng, F., & Effler, S. W. (2011). Characterizations of the light-scattering attributes of mineral particles in Lake Ontario and the effects of whiting. *Journal of Great Lakes Research*, *37*(4), 672–682. https://doi.org/10.1016/j.jglr.2011.07.002

Peng, F., & Effler, S. W. (2017). Characterizations of calcite particles and evaluations of their light scattering effects in lacustrine systems. *Limnology & Oceanography*, *62*(2), 645–664. https://doi.org/10.1002/lno.10451

Perga, M.-E., Maberly, S. C., Jenny, J.-P., Alric, B., Pignol, C., & Naffrechoux, E. (2016). A century of human-driven changes in the carbon dioxide concentration of lakes. *Global Biogeochemical Cycles*, *30*(2), 93–104. https://doi.org/10.1002/2015GB005286

Personnic, S., Domaizon, I., Dorigo, U., Berdjeb, L., & Jacquet, S. (2009). Seasonal and spatial variability of virio-, bacterio-, and picophytoplanktonic abundances in three peri-alpine lakes. *Hydrobiologia*, *627*(1), 99–116. https://doi.org/10.1007/s10750-009-9718-8

Pierrot, D., Lewis, E., & Wallace, D. W. R. (2006). MS Excel program developed for CO2 system calculations. ORNL/CDIAC-105a. Carbon Dioxide Information Analysis Center, Oak Ridge National Laboratory, U.S. Department of Energy, Oak Ridge, Tennessee. https://doi.org/10.3334/CDIAC/otg.CO2SYS_XLS_CDIAC105a

Plée, K., Pacton, M., & Ariztegui, D. (2010). Discriminating the role of photosynthetic and heterotrophic microbes triggering low-Mg calcite precipitation in freshwater biofilms (Lake Geneva, Switzerland). *Geomicrobiology Journal*, *27*(5), 391–399. https://doi.org/10.1080/01490450903451526

Plummer, L. N., & Busenberg, E. (1982). The solubilities of calcite, aragonite and vaterite in CO2-H2O solutions between 0 and 90°C, and an evaluation of the aqueous model for the system CaCO3-CO2-H2O. *Geochimica et Cosmochimica Acta*, *46*(6), 1011–1040. https://doi.org/10.1016/0016-7037(82)90056-4

Ridgwell, A., & Zeebe, R. E. (2005). The role of the global carbonate cycle in the regulation and evolution of the Earth system. *Earth and Planetary Science Letters*, *234*(3–4), 299–315. https://doi.org/10.1016/j.epsl.2005.03.006

Rueda, F. J., Fleenor, W. E., & de Vicente, I. (2007). Pathways of river nutrients towards the euphotic zone in a deep-reservoir of small size: Uncertainty analysis. *Ecological Modelling*, *202*(3–4), 345–361. https://doi.org/10.1016/j.ecolmodel.2006.11.006

Sastre, V., Loizeau, J. L., Greinert, J., Naudts, L., Arpagaus, P., Anselmetti, F., & Wildi, W. (2010). Morphology and recent history of the Rhone River Delta in Lake Geneva (Switzerland). *Swiss Journal of Geosciences*, *103*(1), 33–42. https://doi.org/10.1007/s00015-010-0006-4

Shanableh, A., Al-Ruzouq, R., Gibril, M. B. A., Flesia, C., & Al-Mansoori, S. (2019). Spatiotemporal mapping and monitoring of whiting in the semi-enclosed Gulf using Moderate Resolution Imaging Spectroradiometer (MODIS) time series images and a generic ensemble tree-based model. *Remote Sensing*, *11*(10), 1193. https://doi.org/10.3390/rs11101193

Silva, T. A., Girardclos, S., Stutenbecker, L., Bakker, M., Costa, A., Schlunegger, F., et al. (2019). The sediment budget and dynamics of a delta-canyon-lobe system over the Anthropocene timescale: The Rhone River delta, Lake Geneva (Switzerland/France). *Sedimentology*, *66*(3), 838–858. https://doi.org/10.1111/sed.12519

Sondi, I., & Juračić, M. (2010). Whiting events and the formation of aragonite in Mediterranean karstic marine lakes: New evidence on its biologically induced inorganic origin. *Sedimentology*, *57*(1), 85–95. https://doi.org/10.1111/j.1365-3091.2009.01090.x

Spötl, C., & Vennemann, T. W. (2003). Continuous-flow isotope ratio mass spectrometric analysis of carbonate minerals. *Rapid Communications in Mass Spectrometry*, *17*, 1004–1006. https://doi.org/10.1002/rcm.1010

Stabel, H.-H. (1986). Calcite precipitation in Lake Constance: Chemical equilibrium, sedimentation, and nucleation by algae. *Limnology & Oceanography*, *31*(5), 1081–1094. https://doi.org/10.4319/lo.1986.31.5.1081

Steinmetz, F., & Ramon, D. (2018). Sentinel-2 MSI and Sentinel-3 OLCI consistent ocean colour products using POLYMER. In R. J.Frouin, & H.Murakami (Eds.), *Remote sensing of the open and coastal ocean and inland waters* (Vol. 10778, p. 13). SPIE. https://doi.org/10.1117/12.2500232

Stets, E. G., Butman, D., McDonald, C. P., Stackpoole, S. M., DeGrandpre, M. D., & Striegl, R. G. (2017). Carbonate buffering and metabolic controls on carbon dioxide in rivers. *Global Biogeochemical Cycles*, *31*(4), 663–677. https://doi.org/10.1002/2016GB005578

Strong, A. E., & Eadie, B. J. (1978). Satellite observations of calcium carbonate precipitations in the Great Lakes. *Limnology & Oceanography*, *23*(5), 877–887. https://doi.org/10.4319/lo.1978.23.5.0877

Stumm, W., & Morgan, J. J. (2012). *Aquatic chemistry: Chemical equilibria and rates in natural waters*. Wiley.

Stutenbecker, L., Delunel, R., Schlunegger, F., Silva, T. A., Šegvić, B., Girardclos, S., et al. (2018). Reduced sediment supply in a fast eroding landscape? A multi-proxy sediment budget of the upper Rhône basin, Central Alps. *Sedimentary Geology*, *375*, 105–119. https://doi.org/10.1016/j.sedgeo.2017.12.013

Szramek, K., & Walter, L. M. (2004). Impact of carbonate precipitation on riverine inorganic carbon mass transport from a mid-continent, forested watershed. *Aquatic Geochemistry*, *10*(1–2), 99–137. https://doi.org/10.1023/B:AQUA.0000038960.63501.5b

Thompson, J. B., Schultze-Lam, S., Beveridge, T. J., & des Marais, D. J. (1997). Whiting events: Biogenic origin due to the photosynthetic activity of cyanobacterial picoplankton. *Limnology & Oceanography*, *42*(1), 133–141. https://doi.org/10.4319/lo.1997.42.1.0133

Watkins, J. M., Hunt, J. D., Ryerson, F. J., & DePaolo, D. J. (2014). The influence of temperature, pH, and growth rate on the δ18O composition of inorganically precipitated calcite. *Earth and Planetary Science Letters*, *404*, 332–343. https://doi.org/10.1016/j.epsl.2014.07.036

Zobrist, J., Schoenenberger, U., Figura, S., & Hug, S. J. (2018). Long-term trends in Swiss rivers sampled continuously over 39 years reflect changes in geochemical processes and pollution. *Environmental Science and Pollution Research*, *25*(17), 16788–16809. https://doi.org/10.1007/s11356-018-1679-x